PALEOSEISMIC ANALYSIS OF THE SPRINGFIELD FAULT, CENTRAL CANTERBURY

A thesis

submitted in partial fulfillment

of the requirements for the degree

of

Bachelor of Science with Honors

at the

University of Canterbury

by

STEWART THOMAS EVANS

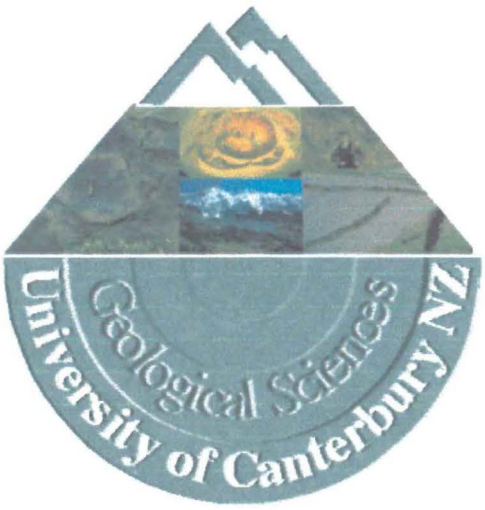

University of Canterbury,

JULY 2000

ABSTRACT

The Springfield Fault is a northeast striking thrust fault bisecting the Russell Range at the northern end of the Malvern Hills near Springfield. The trace of the fault is best expressed by offset river terraces, as it cuts across the flood plane of the Hawkins River in the Upper Hawkins Basin.

The Russell Range is composed chiefly of the basement Triassic rocks of the Torlesse terrane with Cretaceous to Cenozoic rocks occurring in a fault bounded slice and around the hinge of the hanging wall anticline of the fault. Quaternary glacial sediments occur on the plains adjacent to the Russell Range with Holocene deposits occurring in the Upper Hawkins Basin.

Folding in the highly sheared basement is along NW-SE trending fold axes. The current direction of principal shortening was determined from slickenside data to be NW-SE to NE-SW.

Geomorphology of the area in the Upper Hawkins Basin provided a chronology of the activity on the Springfield Fault. Offset of terrace surfaces provide evidence for the number of fault ruptures, which is at least two.

An attempt to date the age of fault and river terrace scarps was made using their morphology and a diffusion model of scarp degradation. Analysis requires the diffusivity rate operating on a scarp to be known to produce an absolute age for the scarp. Only one of the scarps analyzed, a river terrace scarp produced a result. This was poorly constrained at 1000-7500 years old.

ACKNOWLEDGEMENTS

The supervision and assistance of Mrs J. K. Campbell was outstanding. The idea for this project, suggestions of further techniques and ideas, and assistance with autocad were much appreciated. Her vast knowledge of all things geological and her keen eye for subtle geomorphic features are incomparable. The assistance of Dr. J. McKean with scarp degradation models was also much appreciated.

I would also like to thank Michelle Wright and Matt Howard for their assistance with surveying. And all those people who helped to broaden my knowledge of the capabilities of computers.

Thanks to Mason Trust for their assistance with funding

Thanks to the Selwyn Plantation Board for providing access to their property and also up dated maps of their property.

Thanks to all the other landowners for allowing access on to their properties especially those that had to dodge survey marker pegs scattered across their paddocks.

Finally a special thanks to family and friends who have encouraged me whose company I have missed over the past months.

TABLE OF CONTENTS

FIGURES

TABLES

CHAPTER 1: INTRODUCTION

1.1 REGIONAL SETTING

New Zealand lies along the plate boundary between the Pacific and Australian plates. North of New Zealand, along the Kurmedec trench and along the east coast of the North Island west-facing subduction of the Pacific plate below the Australian plate is occurring. Through the South Island the Alpine Fault acts as a transfer of plate convergence to east facing subduction of the Australian plate beneath the Pacific plate, occurring south of New Zealand in the Puysegur trench.

Convergence on the plate boundary along the Alpine Fault ranges from a vector trending 084° at a rate of 45 mm yr^{-1} (Norris *et. al.* 1990) to 071° at a rate of 39 mm yr^{-1} (De Mets *et. al.* 1990), depending on the calculated location of the Euler pole. The oblique nature of the Alpine Fault, striking 055° to the convergence direction, allows the amount of convergence to be resolved into two components, one parallel to the fault of 40 mm yr^{-1} and one perpendicular to the fault of 22 mm yr^{-1} (Norris *et. al.* 1990; Walcott 1979), and 37 mm yr^{-1} and 11 mm yr^{-1} based on the convergence calculation by De Mets and others (1990).

This has resulted in a dextral strike slip separation component of 480 km along the Alpine Fault. Rapid uplift of the Southern Alps to the east is also occurring with rates ranging from 8-10 mm yr^{-1} (Bull and Cooper 1986; Norris *et. al.* 1990). This uplift is accommodated largely by Cenozoic reverse faults which are widespread on the eastern side of the Alpine Fault (Fig 1.1).

The Marlborough Fault System in the northern South Island transfers the convergent motion from subduction along the Hikurangi Trough to the zone of crustal thickening and uplift along the Alpine Fault. This is achieved by a series of NE-SW orientated dextral strike slip faults that splay from the Alpine Fault and extend out to the coast.

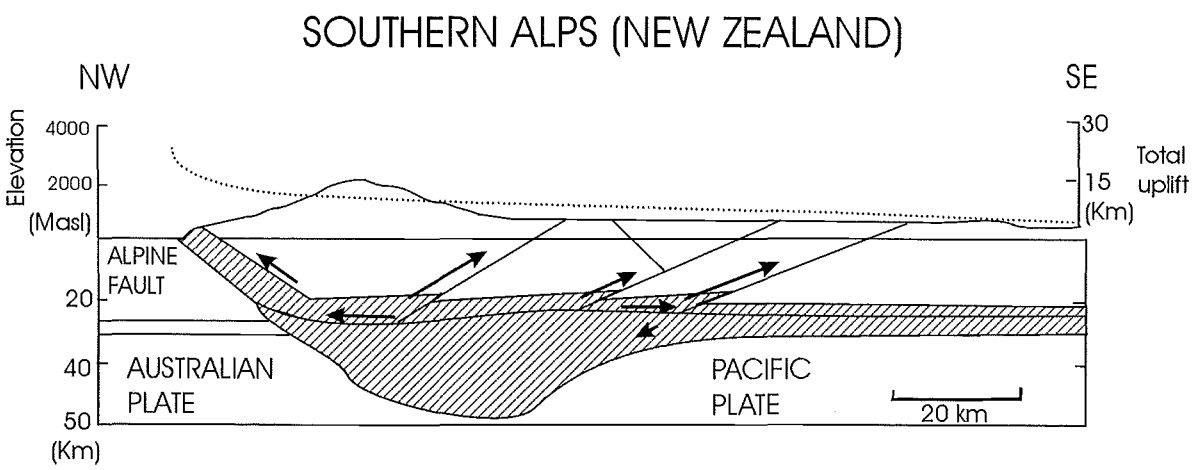

Figure 1.1. Schematic of the two sided deforming wedge model representing the oblique continent-continent collision zone of the Australian-Pacific plate boundary across the central South Island. Amount fo uplift is indicated across the top of the diagram. Modified from Norris *et. al.* (1990).

Deformation in North Canterbury, south of the Marlborough Fault System, is dominated by NE striking range front, reverse and thrust faults with associated folding. This regional trend is reflective of the NW-SE compression that is dominant in the region (Nicol and Wise 1992).

The Springfield Fault is located just south of the hybrid strike slip and thrust faulted Porters Pass to Amberley Fault Zone, which is thought to be a developing strike slip system similar to those in the Marlborough Fault System. The Springfield Fault is positioned in this domain, Domain 3, on the boundary with the northeast striking thrust and reverse faults of Domain 5 (Pettinga *et.al.* 1998) (Fig.1.2) to the south. The boundary is not well defined, but the Springfield fault is positioned in Domain 3 rather than Domain 5 because it dips to the southeast like many of the thrust and reverse faults in Domain 3 compared to the west facing thrusts and reverse faults of Domain 5, the zone of major range front faults in Mid and South Canterbury.

The Springfield fault is most likely related to the nearby Kowai Fault to the North, with both structures dipping to the southeast.

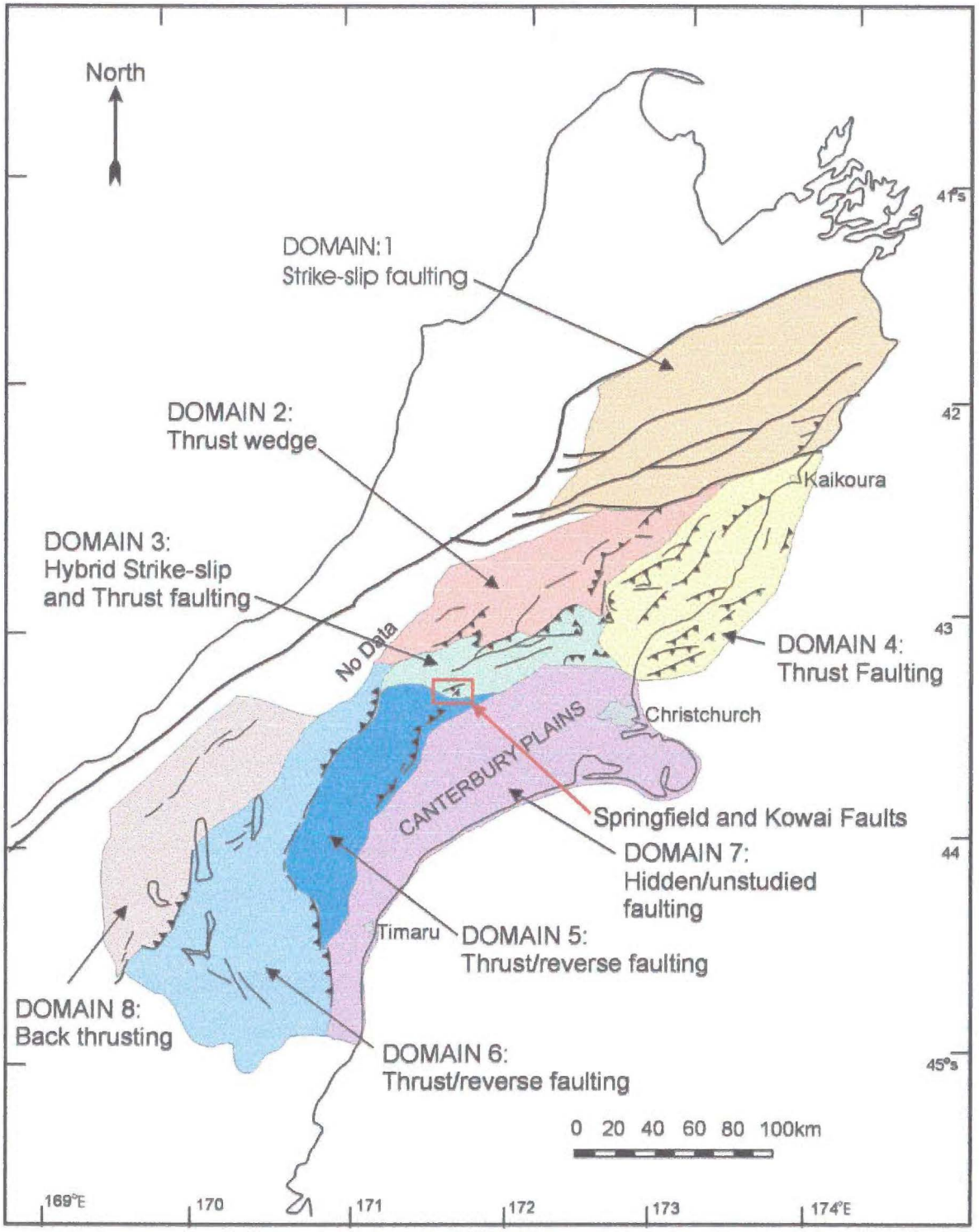

Figure 1.2. Summary map of the 8 structural domains of the Canterbury region (Pettinga *et. al.* 1998)

1.2 LOCATION OF STUDY AREA

The study area is located at the eastern end of the Russell Range, southwest of Springfield central Canterbury. The southern boundary of the area is the north side of the Selwyn River and the northern boundary is State Highway 73 and Springfield township. The west boundary runs northeast from the North Branch Selwyn River, where a rain gauge is located, to State Highway 73, skirting the lower slopes of Russell Peak on the way. The east boundary runs from the lower eastern slopes of Bell Hill to State Highway 73 in the northeast.

The majority of the area is drained by the Hawkins River flowing to the east through an open valley, dubbed the Upper Hawkins Basin, in the middle of the study area, exiting via a low gorge to the Canterbury Plains. The major peaks are Bell Hill (971 m), Russell Peak (941 m) and another peak in the Russell Range labeled F No2 (833 m) on the topographic map (L35).

The Upper Hawkins Basin has often been referred to as Dalethorpe because of 'Dalethorpe' station, which was the last farm on the road into the area and most likely once occupied most of this area. It should be noted that the Dalethorpe station name that appears on topographic maps has been changed, to 'Baldoon'.

Access into the Upper Hawkins basin area is via Dalethorpe Road with numerous tracks extending beyond its end even as far as through to the High Peak Valley to the south. Access to the rest of the study area can be made from either State highway 73 or Springfield Road.

The topography of the study is variable from steep slopes of the Russell Range and Bell Hill, to the flat topography of the gravel surface of the Canterbury Plains. Exposure is generally poor in undisturbed ground, but numerous farm and forestry road cuts provide good exposures.

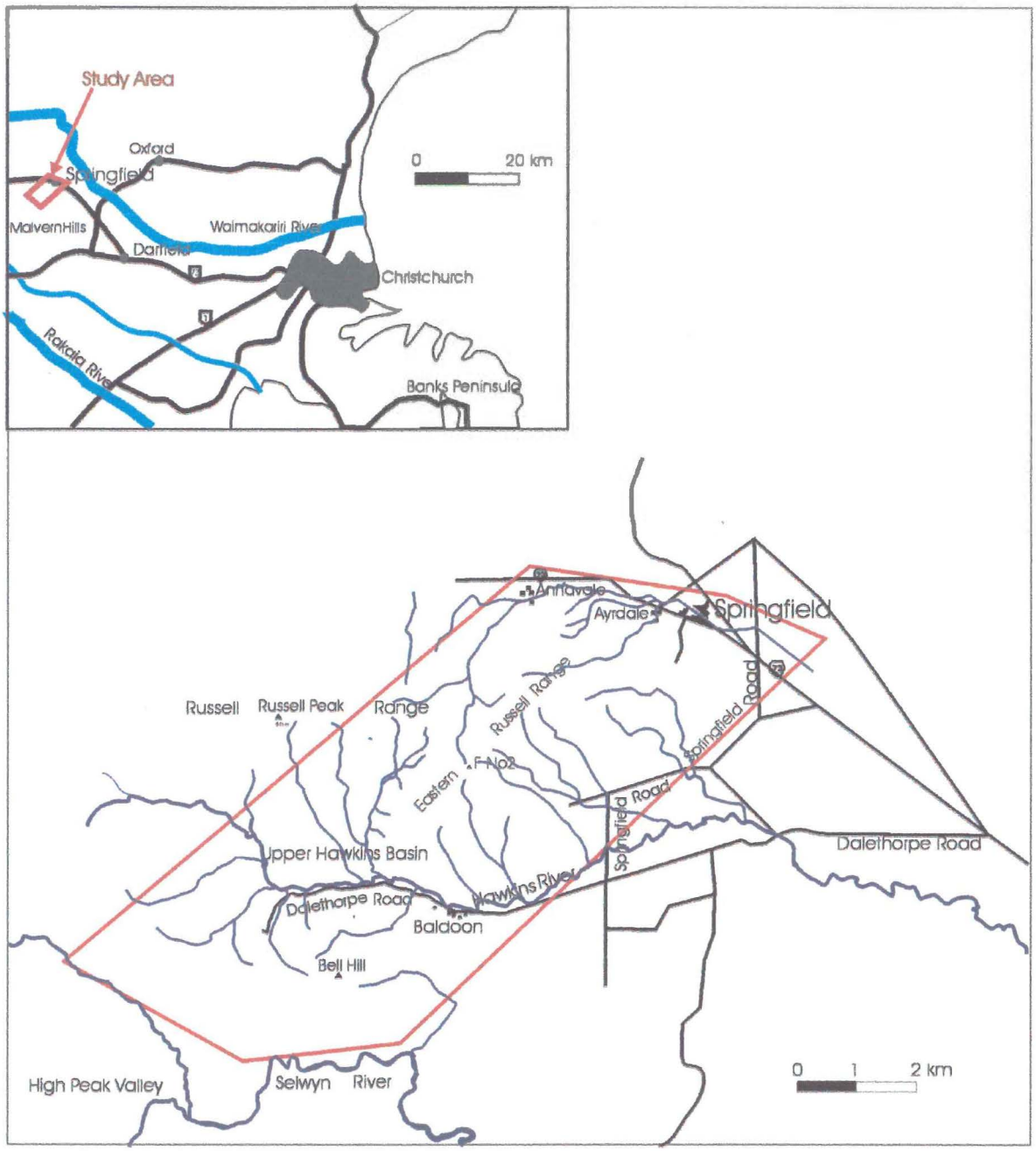

Figure 1.3. Location map of the study area showing major roads, rivers and landmarks.

1.3 OBJECTIVES

Three main objectives are set out for this project;

(1) Map out the Springfield Fault and associated propagating anticlinal structure.

(2) Determine the Kinematics of deformation operating in the study area.

(3) Implement and compare fault scarp degradation models, which have been proposed as methods of dating fault scarps and evaluate the practicality of using these methods for dating displacement events.

General geological mapping and the collection of fault slip data were carried out during January (2000). Detailed topographic surveying was carried out during February and March (2000) along with further collection of fault slip data.

Mapping was carried out on N.Z.M.S. 260 series, Sheet L35 Waimakariri, with the aid of N.Z. Aerial mapping Ltd. air-photo runs, 3706 1-5, 3705 1-2. All geographic locations are on Sheet L35 or the locality map.

1.4 PREVIOUS WORK

Early work in the Malvern Hills area was undertaken by Hector (1871) and von Haast (1871 and 1872). Von Haast (1872) mentioned the Springfield and Hawkins River area, but made no mention of identifying coal measures at Springfield or near Dalethorpe.

The next formal writing on the area consists of reports on the Springfield Colliery (Cox 1884a and 1886; Lindop 1884 and 1886), outlining projected coal reserves, exploration and mine development. Cox (1884b) documents the Jurrassic beds in the upper Selwyn Valley indicating their continuation through to the Hawkins valley.

The first mention of the Springfield Fault is made by Speight (1924), along with the isolated outcrop of coal measures adjacent to it. Speight also suggests that the Upper Selwyn River possibly flowed into the Hawkins River.

Speight (1928) provides the most thorough account of the geology of the Malvern Hills. A good account of the Cretaceous geology around Springfield is made. The outlier of Cretaceous rocks adjacent to the Springfield Fault at Dalethorpe is also mentioned in detail. The relationships of units are well constrained by Speight (1928), possibly owing to better exposure as a result of mining in the area.

Since Speight (1928) there has been very limited formal written work on this particular area of the Malvern Hills. Geological maps of the area include the N.Z.G.S. 1:250 000 series, Sheet 18, Hurinui by Gregg (1964), and a map of the Quaternary geology of northwestern Canterbury Plains (Wilson 1988). Wilson (1988) summarizes the entire geology of the Malvern Hills area, giving a detailed account of the Quaternary geology.

Other work has been carried out on the Quaternary geology of the Malvern Hills area although none has really covered the area of this study. Rains (1967) covered the Pleistocene geology of the High Peak Valley to the south of the Upper Hawkins Basin. Marden (1976) covered the Late Pleistocene geology of the Kowai River Valley to the northwest of the area covered in this study. Both works discuss glacial geology that is relevant to the area of this study, including the influence of glaciation in the Upper Hawkins Basin (Rains 1967) and glacial deposits around the Springfield area (Marden 1976).

CHAPTER 2: STRATIGRAPHY

2.1 BASEMENT ROCKS

The basement of the area consists of Torlesse Rakaia Terrane of Jurrasic-Lower Cretaceous age, being of *Torlessia* fossil zone (Late Triassic) in the Malvern Hills area (*Andrews et. al.* 1976). It is characterized in this area by interbedded sandstone and mudstone turbidites, with sandstone beds varying in thickness up to ~5m thick. There is also the occasional lensoid shaped bed of red chert, some of silty nature. Bedding is generally orientated at a high dip angle with variations in strike, dominated by a north-northwest, south-southeast strike direction.

Deformation of the Torlesse terrane rocks has occurred during two orogenic episodes (Bradshaw 1971). The earlier Rangitata Orogeny is separated into two phases, a Jurassic Rangitata I and Cretaceous Rangitata II phase (Bradshaw *et .al.* 1980). The Rakaia terrane Torlesse rocks are affected by both episodes. This deformation produced the sub-vertical fold axes with steeply dipping fold limbs (65-90°) that gives the Torlesse terrane rocks found in the Canterbury region a characteristic steeply dipping to overturned orientation of beds. Low-grade metamorphism occurred during this orogeny.

The younger Kaikoura Orogeny is indicated by the folding and faulting of the Cenozoic rocks along with the Torlesse basement rocks of the Canterbury region. This has produced a different style of deformation to the Rangitata Orogeny, dominated by pervasive fracturing, major brittle shear zones and faults.

2.2 CRETACEOUS TO CENOZOIC ROCKS

The Cretaceous to younger rocks are located in the small hills to the southeast, behind Springfield township, and in a small fault controlled outcrop approximately 40m wide at its maximum and 500m long located in the valley of a true left tributary of the Hawkins River, in the Upper Hawkins Valley. The Cretaceous rocks are Eyre group Broken River Formation and View Hill Volcanics.

2.2.1 BROKEN RIVER FORMATION

The Broken River Formation in this area is generally poorly represented in outcrop, possibly due to the easily eroded nature of some units. Its main identifying feature is the presence of coal.

Float rocks of well-indurated ferruginous sandstone and the occasional holes in the ground revealing coal fragments in the soil are generally the only indication of Broken River Formation, where the topography is low and not cut by streams. This may account for the failure by early workers (Hector 1871; von Haast 1871 and 1872) to report potential coal resources, especially around Springfield. The historical evidence of coalmines such as air tunnels, shafts, supporting timbers and building ruins also serves to indicate the likely location of the coal bearing Broken River Formation where little or no surface outcrop now occurs.

Outcrop of the other Broken River Formation lithologies is limited to the fault-bounded outcrop located on the tributary of the Hawkins River and to roadcuts on the small hills to the southeast of Springfield. Two stream cuts through the fault bounded outcrop (L35 176594 and 178598) reveal poorly indurated lignite coals and clays, as well as scree containing higher quality coal and float rocks of dark slate.

Between these two stream cuts, isolated, *in situ* outcrops of the well-indurated ferruginous sandstone occur. This sandstone appears to underlie a silty sandstone that is probably poorly indurated as the evidence is only by preservation in bioturbated casts in the upper part of the well-indurated ferruginous sandstone. These sandstones are stratigraphically below the coal units. The contact with the underlying Torlesse Basement is uncertain due to poor outcrop, but is likely to be faulted, at this locality. Normally the Broken River Formation would lie on a deeply weathered unconformable contact with basement Torlesse rocks.

Higher quality altered coal is also observed in the stream bank, in what is assumed to be a spoil heap from the coal mine that operated there, as indicated by timber nearby. Speight (1928) noted a similar occurrence. Alteration is likely to be from pressure caused by faulting, as suggested by Speight (1928).

The orientation of bedding is variable in the limited outcrops, ranging from a dip of 25° to the SE, to 15° to the NE into the hill beneath overthrust Torlesse Basement. This is similar to the values obtained by Speight (1928) from within the coalmine drive of a dip of 20° to the SE.

Roadcuts at the Springfield location of Broken River Formation reveal lignite coal seams one meter thick, as well as highly weathered quartz sands with flecks of carbonaceous material and gray laminated mudstones. Bedding here is orientated along a strike of approximately 120° dipping 20° to the northeast. These are overlain by the View Hill Volcanics.

2.2.2 VIEW HILL VOLCANICS

The Eocene aged View Hill Volcanics (Andrews *et.al.* 1987) occur in the low hills to the southeast of Springfield. Float rocks are widespread suggesting a more widespread distribution than there is. They are dolerite flow rocks interpreted as a sill by Speight (1928), who commented on the lack of exposure of the contact with the underlying Eyre group that makes interpretation of the general area difficult. Recent roadcuts in the area reveal the contact with the underlying Broken River Formation. Here the coal and sand-silt beds are altered, by baking, for approximately 70-100 cm below the contact. Unfortunately though there is no upper contact revealed for the volcanics making an interpretation between sill or lava flow difficult. The apparent thinness of the older, Cretaceous sequence that underlies the volcanics adds weight to the interpretation as a sill.

Speight (1928) calculated a maximum thickness of the View Hill Volcanics from borehole data of Cox (1886) and Lindop (1886) of 200 ft. (60 m). Much less than this is revealed in out crop, although faulting may complicate the situation.

COMPOSITE STRATIGRAPHY OF THE EASTERN RUSSELL RANGE AND UPPER HAWKINS RIVER VALLEY BASIN

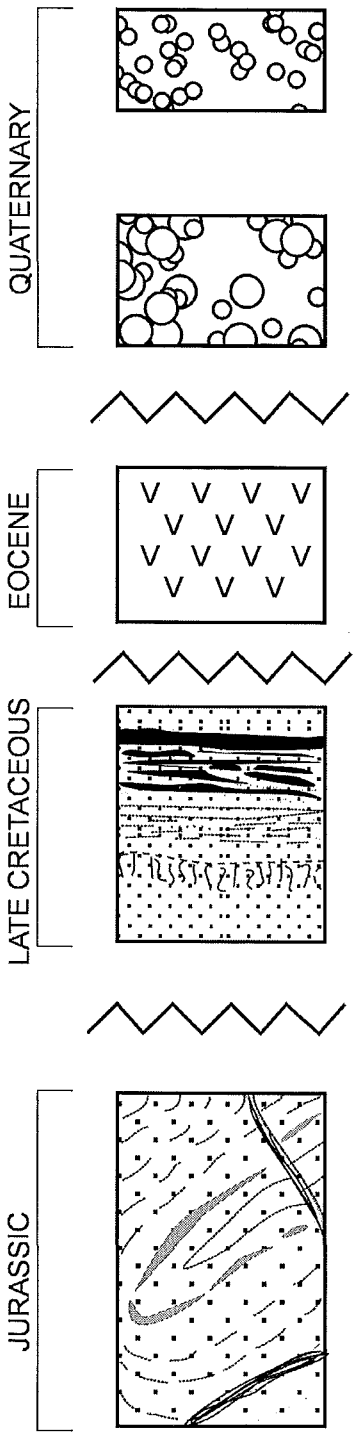

RECENT DEPOSITS

Alluvial fans, river deposits scree slopes soils and swamp deposits.

GLACIAL AND FLUVIOGLACIAL DEPOSITS

Woodlands, Windwhistle and Springston Formations, incompassing two glacial advances, Waimea and Otirian. Out crop is poor with relationships being infered from geomorphological relationships and work of Wilson (1988).

VIEW HILL VOLCANICS

Grey, well indurated dolerite. prominant altered red olivine and feldspar. In places there is a layering in the rocks. Outcrop is generally poor with the extent coverage being indicated by numerous areas of well indurated float rocks.

BROKEN RIVER FORMATION

Well indurated ferruginous sandstone with numerous burrows, near the base of this formation. Brown coal beds with unknown relation ship with underlieing units.Float rocks of dark slate and higher quality coal. Bedding approximately dipping 20 degrees to the east.

TORLESSE TERRANE ROCKS

Rakaia Terrane. Interbedded Greywacke and Argillite. Well indurated quartzofeldspathic sandstones and siltstones, massive sandstone beds up to 5m, occasional lensoid shaped bedded chert. Metamorphosed to zeolite facies, sub-vertical bedding and highly sheared.

Figure 2.1 Composite and schematic stratigraphic column of the Springfield and Russell Range areas. Dates are from Wilson (1988) and Andrews *et.al.* (1987).

2.3 QUATERNARY GEOLOGY

Quaternary geology within the study area consists of Woodlands and Windwhistle Formation glacial gravels, and the fluvial reworkings of these glacial gravels, the Springston Formation (Wilson 1988). Other deposits include scree, recent fluvial flood plain and degradation terrace deposits. The glacial and reworked glacial deposits are limited to the areas of low topography to the east and north of the study area. The remaining area only has Holocene deposits, which are localized and not assigned formation names. Due to thick cover of soil and low topography the Quaternary formations are generally poorly exposed.

The Woodlands Formation is the oldest Quaternary gravel in the study area, being deposited during the Woodstock advance of the Waimakariri glaciers during the Waimea Glaciation (Brown and Wilson 1988; Wilson 1988). It occurs south east of the Cretaceous rocks at Springfield and along the south bank of the Lower Hawkins River Basin (Wilson 1988). A pronounced terrace scarp 2-3 m high extends from the northern end of the small hills behind Springfield, produced by the View Hill Volcanics, and runs ESE with decreasing scarp height until it joins the level of the younger Windwhistle and Springston Formations.

The Windwhistle Formation was deposited during an early advance of the Otiran glaciation (40-70 000 BP)(Wilson 1988). It occurs along the eastern edge of the older Woodlands Formation southeast of Springfield and forms the dominant surface that extends eastwards along the Waimakariri River.

The Springston Formation consists of fluvial reworked, earlier glacial deposits. These deposits occur to the north and east of the study area, representing the location of the Hawkins and Kowai river systems during the last 10 000 yrs (Wilson 1988). The Woodlands Formation has been reworked by runoff from the Russell Range in a triangular shaped area between the hills southeast of Springfield and the Hawkins River to the south. Here the morphology of the gravels surface is rough and channeled unlike the generally even surface of the Woodlands Formation. The Springston Formation also occurs to the north and east of Springfield as the channel once occupied by the Kowai River that can be

traced passing north of Springfield and then curving around to join the similar formation produced by the Hawkins River.

There is no evidence of glacial deposits within the Upper Hawkins Basin upstream of Dalethorpe. Here the Quaternary geology consists of alluvial fans, scree slopes and degradation river terraces. The degradation river terraces preserve the story of deformation and uplift along the Springfield Fault and the response of the Hawkins River to it.

Because there are no glacial deposits within the Upper Hawkins Basin does not mean the basin was not affected by glaciation. The low saddle to the south separating the basin from the glaciated High Peak valley and upper Selwyn River catchment, appears to be the ideal location for glacial ice to have spilled over from the Rakaia glaciers. Speight (1928) envisaged this occurring during the older of the two recorded advances of the Rakaia glaciers into the High Peak Valley, the Woodlands advance (equivalent to the Woodstock advance of the Waimakariri glaciers)(Rains 1967). This advance is poorly constrained with no record of the glacier's terminus remaining preserved. Rains (1967) suggests that an earlier, larger, glaciation equivalent to the Avoca Glaciation in the Waimakariri valley may have occurred in the High Peak Valley. If the Woodlands advance did not reach through from the High Peak valley into the Upper Hawkins Basin the Avoca Glaciation is likely to be responsible for the low saddle.

CHAPTER 3: STRUCTURE

3.1 STRUCTURE OF THE TORLESSE BASEMENT ROCKS

The structure of the Torlesse Basement rocks inherited from the Mesozoic is generally complex, with tight upright isoclinal folds being prominent. Due to the lack of outcrop and the numerous shear zones within the study area it is difficult to trace prominent beds, such as chert beds, to interpret the large-scale structure of the basement, as was done by Bradshaw (1971) and Coyle (1988). Despite this a general north to northeast strike orientation and a steep dip can be inferred from prominent outcrops of sandstone beds along ridge tops and the orientation of beds at outcrop scale.

Shear zones are very abundant throughout the Torlesse Basement. There are generally four types of shears found within the study area:

(1) Bedding parallel shears, which occur in argillite beds that become highly sheared with a clay gauge layer forming along the contact with the sandstone beds, indicating the main location of movement. Slickensides are rare along this shear.
(2) Large shear zones 1 m+ in width. Generally form where numerous argillite beds occur with thin sandstone beds. Zone contains mainly clayey fault gauge with blocks and lenses of sandstone. Slickensides are only present within the sandstone blocks and lenses.
(3) Small, short shears which crosscut bedding, being most obvious in sandstone beds. Generally have small displacements along them. They are the main sources for slickenside data.
(4) Extensive shears that cross bedding at high angles. These are much longer with a greater offset than (3). Fault gauge of up to 10 cm occurs. Shears are a good source of slickenside data, especially where the gauge is thin.

Shears in the Torlesse terrane basement rocks do not appear to be limited to within close proximity of major faults but instead are spread throughout the whole basement with higher concentrations located close to major fault traces. This is representative of the deformation mechanisms that are operating in the Torlesse rocks allowing their deformation, even up into the hinges of late Cenozoic folds. The fracturing and shearing allows small discrete blocks to move independently within the mass of basement and fold (Wibberley 1997). The shears predominate along the bedding planes and in the argillite beds, as they are the weakest planes. Small movements on numerous planes can achieve large-scale deformation.

The bedding orientation of the Torlesse rocks is dominated by a northeast strike direction and has a steep dip that varies between northeast and southwest. Plotting of the bedding data on a stereonet reveals that most of the data falls along a NE-SW striking great circle and a second much less significant east-west striking great circle (Fig. 3.1). This confirms that the orientation the fold axes is dominantly NW-SE with a general plunge moderately towards the southeast. The contoured data set suggests that maybe a small circle would fit the data better, but this would only be slightly smaller than a great circle, which shows enough detail.

The second great circle that the poles to bedding fall on is minor compared to the first and is strangely almost perpendicular to the main population of bedding. It is possibly related to a block of the basement that may have been rotated by faulting or late Cenozoic folding.

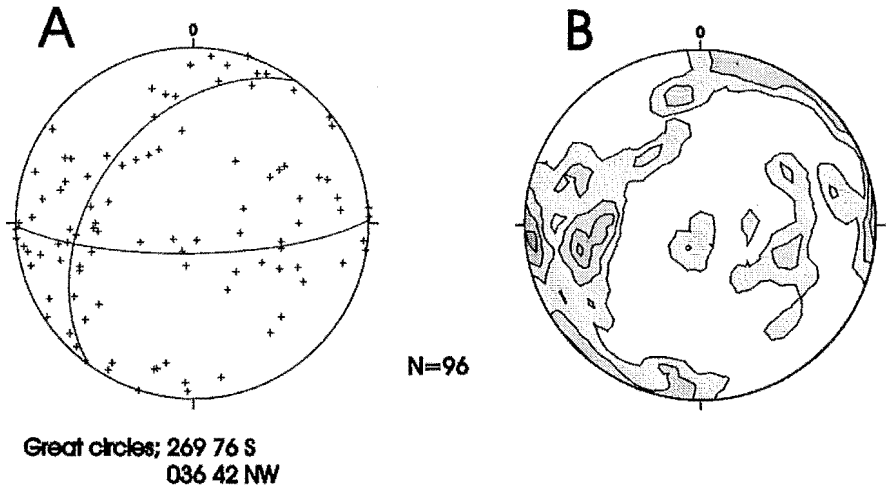

Figure 3.1. Poles to bedding plotted on a stereonet for the entire area, *A*, with two great circles drawn to show major axes of folding. *B*, shows the same data set contoured.

3.2 CENOZOIC STRUCTURE

The dominant Cenozoic structures in the Canterbury region consist of NE-SW trending folds and thrust faults. This pattern continues through the Malvern Hills area. The western Russell Range is bordered to the north by the Kowai Fault, with the range presumably being produced by a hanging wall anticline. This structure possibly includes the whole of the Russell Range with the Springfield Fault being a secondary hanging wall thrust.

3.2.1 THE SPRINGFIELD FAULT

The Springfield Fault is an east dipping thrust fault that has thrust up the eastern end of the Russell Range creating the Upper Hawkins Basin and preserving the small location of Cretaceous rocks there. Along the east facing slopes of the eastern Russell Range the Torlesse terrane rocks are highly weathered indicating close proximity to the Cretaceous unconformity surface (Fig 3.2). The apparent uniformity of the ridge attitude and altitude as well as the rounding and lack of outcrop on these ridges, and the close proximity to the

Cretaceous rocks at Springfield suggests that this surface is the unconformity from the Cretaceous with the Cretaceous rocks eroded off. This means that these slopes are a datum surface that indicates the nature and degree of deformation that has taken place in the Cenozoic.

Figure. 3.2. View looking south towards Bell Hill in the distance from near Springfield. Two sets of arrows indicate surfaces which are underlain by weathered Torlesse and are assumed to indicate the stripped off cretaceous unconformity.

Structural contours can be drawn around the east facing slopes of the Russell Range and continued around to the west of Springfield (Fig. 3.3). This allows a northeast plunging anticline to be recognized going under Springfield, with a small area of Cretaceous rocks and View Hill Volcanics outcropping around the axial hinge of the anticline. The Cretaceous rocks undoubtedly continue under Russells Flat and to the west beneath the Kowai Valley, which is supported by the observations of Speight (1928) of Cretaceous sediments near the State Highway 73 bridge across the Kowai River to the northwest of the study area.

To the west of Springfield the apparently simply interpreted fold structure would be expected to be complicated by the Springfield Fault. Surprisingly its influence is apparently absent. The fault could not be traced any further than just beyond the saddle at the head of the valley of the tributary where the fault bounded outcrop of Broken River Formation occurs (L35 190610). Generally flat ground on top of the hills 1-2 km to the northeast (L35 205625) of this location appear to indicate the footwall of the fault which would then run approximately along the stream that flows down past the 'Ayrdale' homestead and then through Springfield township and across towards the Waimakariri River (Wilson 1988). Instead the displacement on the fault appears to decrease along its length towards the northeast. This is supported by the unweathered nature of the rocks in the hill between the 'Ayrdale' and 'Annavale' Homesteads when if large displacement equivalent to that occurring in the Upper Hawkins Basin would have resulted in the Cretaceous unconformity surface being below that on the hanging wall and possibly have produced outcrops of Cretaceous Rocks along the front of this hill.

A likely explanation for the structure at the end of the traceable, trace of the fault is a splaying of the fault with the displacement being taken up on several fault strands possibly running down the courses of some of the streams that drain out towards 'Annavale' and 'Ayrdale'. This has possibly caused the elevation of the flat ground on the top of the hills, presumed to be the reference Cretaceous erosion surface mentioned above, up above the relative altitude we would expect it to be at. A possible explanation, of the mechanism operating here, is that the interference of the anticlines produced by the Kowai Fault and the Springfield Fault causes the Springfield Fault to splay.

A cross-section drawn of the Springfield Fault indicates that the idea of the Springfield Fault being a second-generation structure to the Kowai Fault might be correct (Fig. 3.4). The Springfield Fault appears to break up through the hanging-wall anticline associated with the Kowai fault.

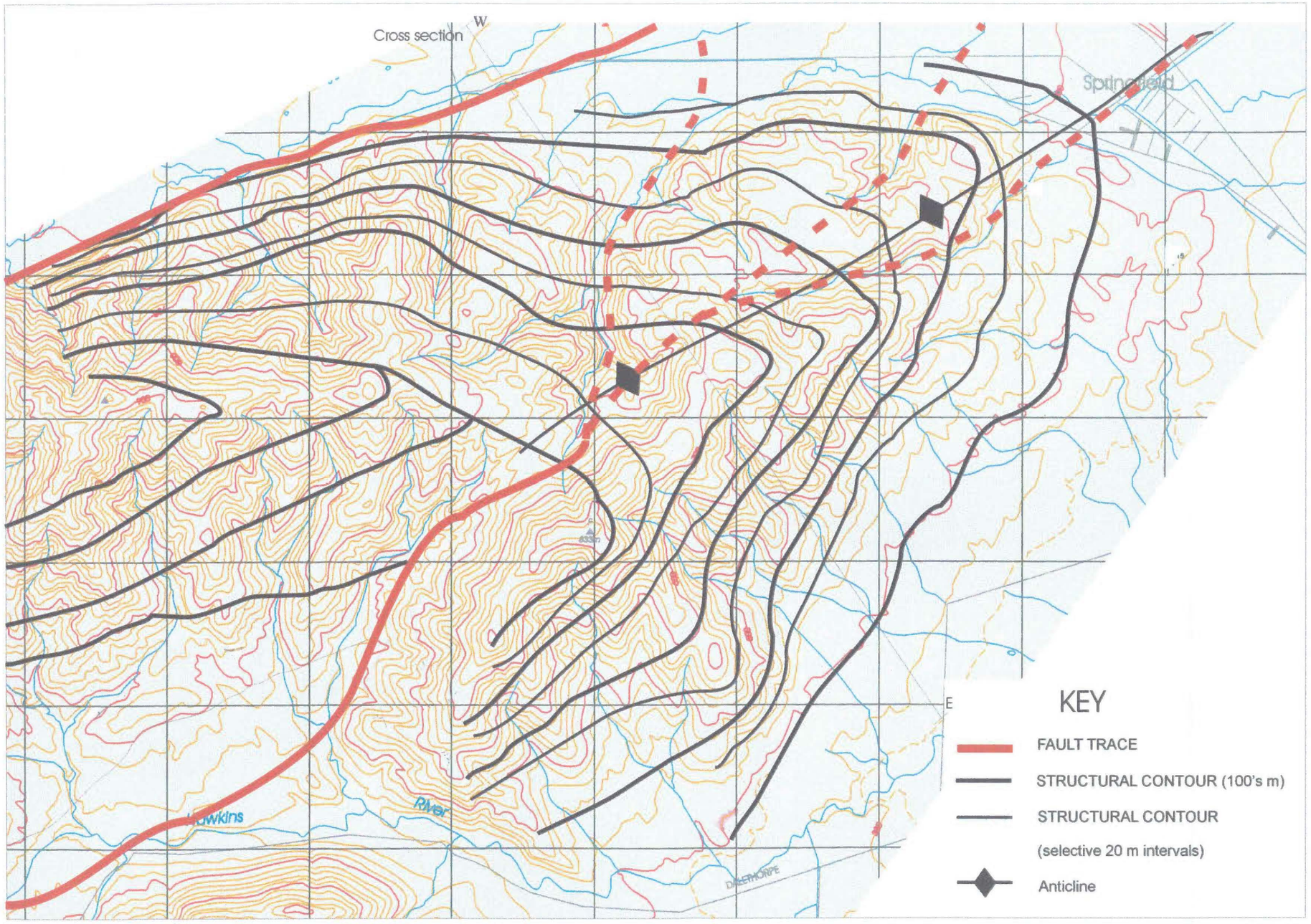

Figure 3.3. Map of the study area with inferred structure contours drawn on the Cretaceous unconformity by joining topographic contours of the same heights where they are least altered by erosion on the tops of spurs.

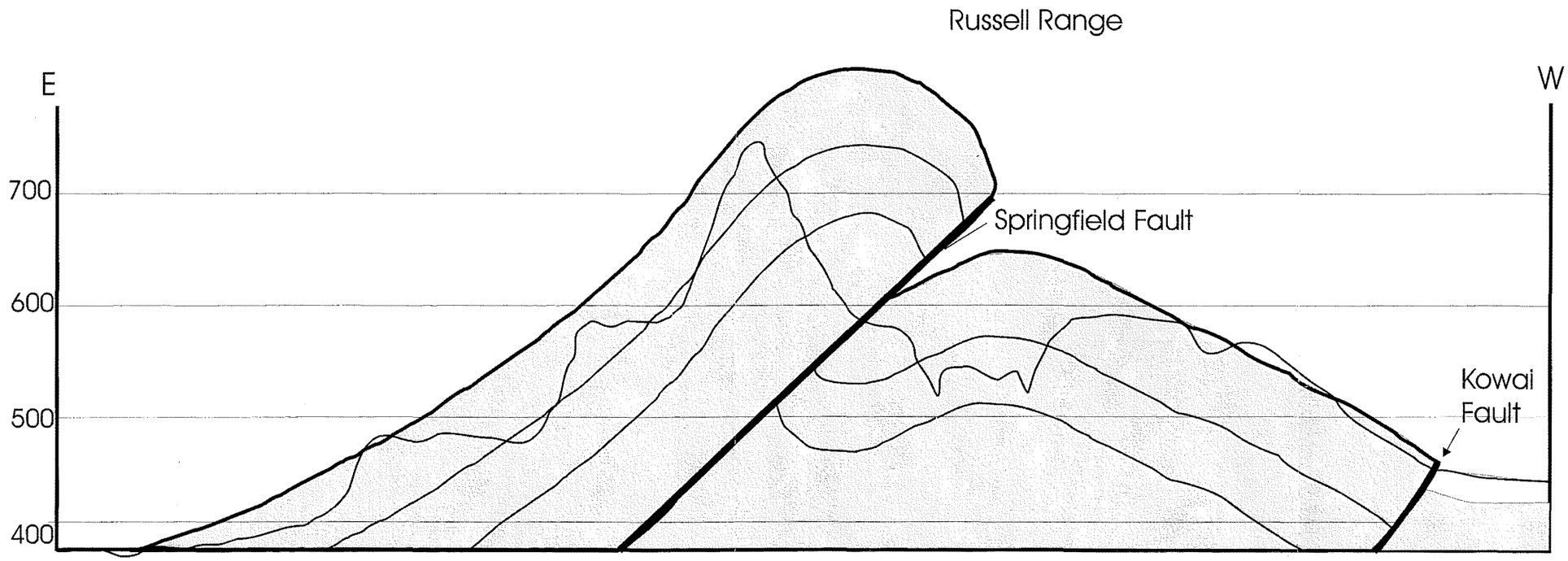

Figure 3.4. Probable cross section of the Springfield Fault, with surface shown being the Cretaceous unconformity. Drawn along the section line shown on shown Fig.3.3, derived from the structural contours in Fig. 3.3. Topography is shown with no amount of displacement shown on the Kowai Fault. Vertical exaggeration of 1:40.

3.2.2 OTHER FAULT TRACES

There were several other fault traces located within the study area. One was located on the northwest face of Bell Hill about half way up and is likely to be partially responsible for the steep topography on this face. It is a thrust fault of orientation not too dissimilar to that of the Springfield Fault and possibly could be related to it, or the uplift of the range of hills to the east of Bell Hill.

Several linear features were noted on the series of aerial photos but further exploration on the ground failed to identify these as fault traces for certain. This was mainly due to the poor quality of outcrop, which was intermittent making structures difficult to trace, with broad shear zones occurring frequently, and often where there had been no linear features identified. Most linear features turned out to be a result of erosion, especially involving the steeply dipping, prominent sandstone beds, which formed linear strike ridges across the topography.

CHAPTER 4: DETERMINATION OF PRINCIPAL STRESS AXES

4.1 INTRODUCTION

The analysis of the paleo-stress indicators to determine the stress regime active within an area is useful for understanding the orientations and attitudes of recent fault and fold structures. It is most effective where rocks have been subjected to a single stress regime such as the Cenozoic rocks of Canterbury. Analysis of the Torlesse terrane rocks is complicated by the reactivation of old Mesozoic structures under the new Cenozoic stress regime.

Minor fault orientations and slickenside data was collected from two sites on Bell Hill where good exposure of the sheared and fractured Torlesse terrane rocks occurred in roadcuts. The first site (L1), on the northwest flank of the hill along the forestry road (L35 157573 to 164576), is situated in the area on the hanging-wall of a thrust fault that skirts the northwestern face of the hill (Fig.4.1). A series of outcrops occur in a roadcut just above this fault, providing fresh outcrop of both weathered and non-weathered rock. The second site is on the southwest side of Bell Hill close to the location of an east-west fault mapped by Wilson (1988) that was not located in this study. These outcrops are in road cuts along the forestry road here (L35 156563 to 157559). This area is deformed in a similar manner to the Torlesse terrane rocks in the general area of Bell Hill and along the trace of the Springfield Fault.

Fault and slickenside data was plotted on the computer program StereoNett version 2.40. This allowed the easy manipulation of the data using the m-plane method and provided helpful contouring of the data.

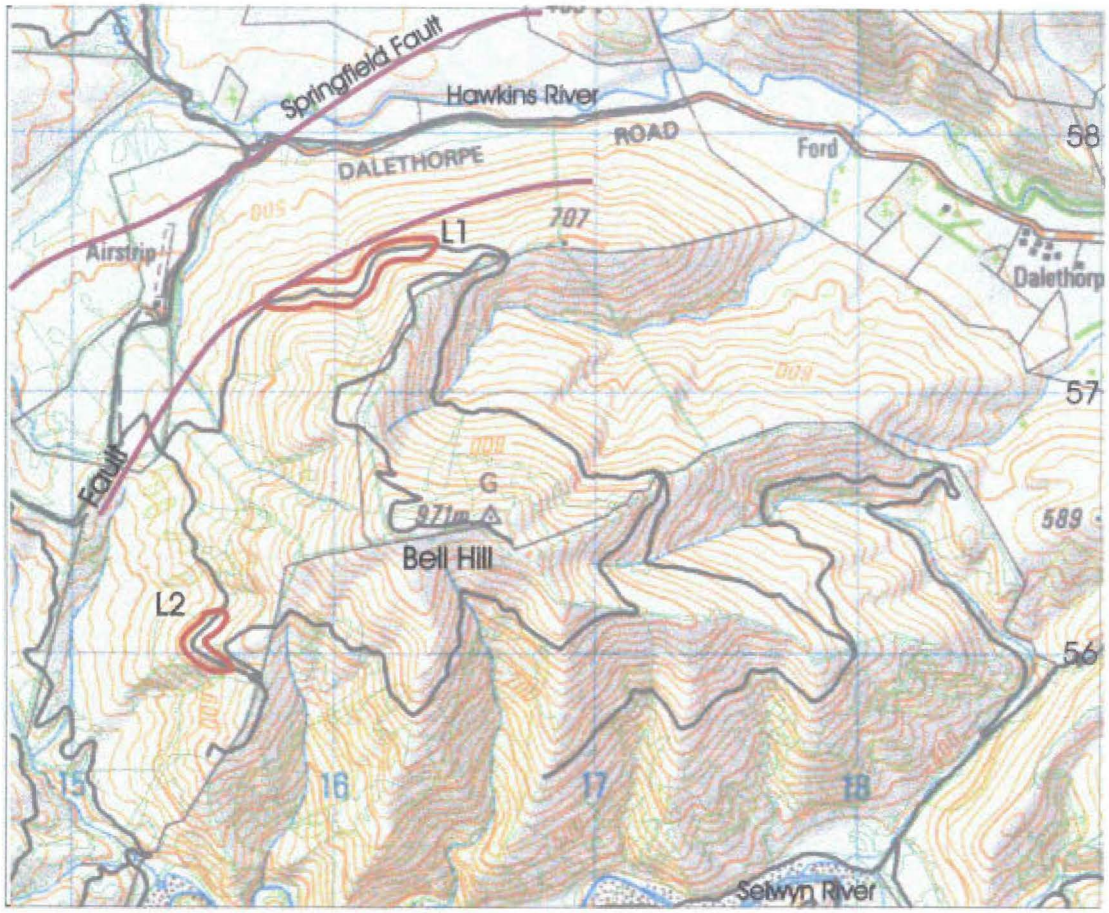

Figure 4.1. Topographic map of Bell Hill with the two locations where the main collection of slickenside data was made and the positions of these locations relative to the local geology.

4.2 M-PLANE METHOD

Movement planes (M-planes) can be used graphically to determine the orientations of the three principal stress axes. M-plane methods rely on the assumption that the intermediate stress axis (σ_2) lies within the fault plane and plays no part in the formation of the slip vector. The maximum (σ_1) and minimum (σ_3) principal stress axes therefore lie within a plane that is perpendicular to the fault plane and parallel with the direction of movement on the fault equivalent to the slickenside orientation (Fig 4.2). The M-plane is represented on a stereographic net as a plane that has on it the slickenside lineation and the pole to the fault plane. The M-pole is the pole to this plane.

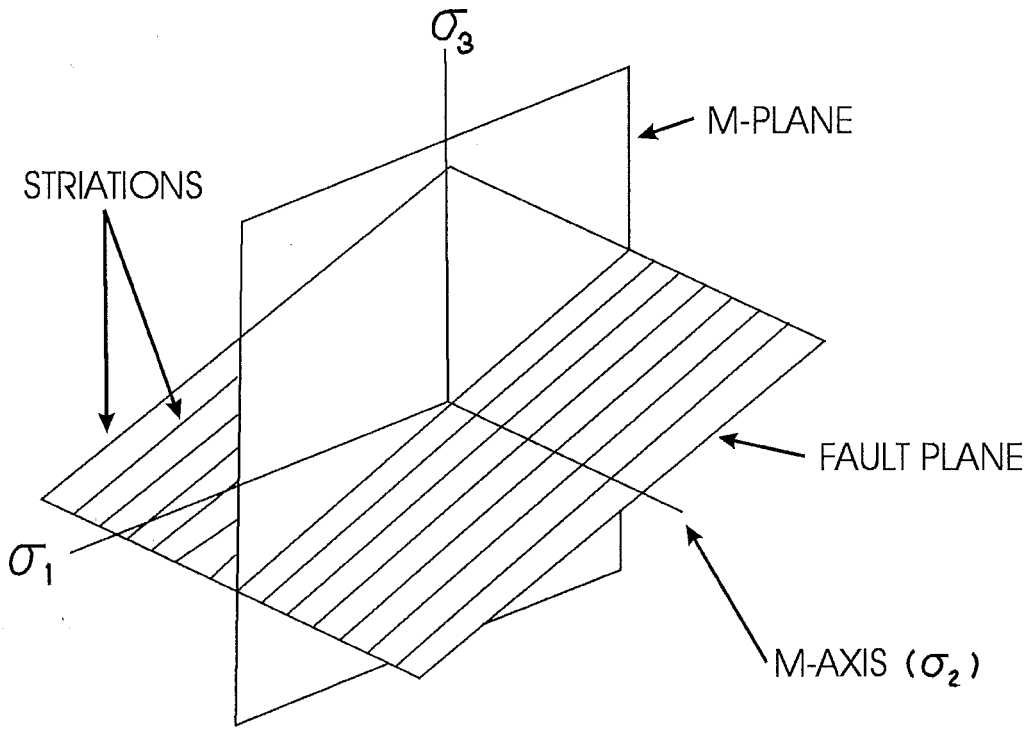

Figure 4.2. A schematic drawing of the fault plane of a reverse fault showing the M-plane containing sigma 1 and 3 parallel to the slickenside stiations and sigma 2 parallel to the fault plane (After Nicol and Campell, 1990).

The method of Arthaud (1969) involves the plotting of M-planes, resulting in them intersecting at a one to three points, which correspond, as poles, to the same number of great circles formed by the M-poles. These points define the deformation axes (only indirectly related to the related to the principal stresses), which indicate directions of maximum shortening, maximum extension and intermediate deformation. The advantage of this method is that it does not require the motions of the slickensides to be known. A disadvantage is that this method can only be applied successfully to slickenside populations that originated in radial (axial) stress fields.

Aleksandrowski (1985) modified Arthaud's method (1969) to be applicable to a general, triaxial stress state, as well as a radial (axial) stress state. This method involves the separation and analysis of separate, common intersection points (CIP) between M-planes. If at least three fault planes corresponding to intersecting M-planes lie on a great circle, the intersection between this great circle (GCF) and a single great circle formed through the M-poles of the intersecting M-planes (GCP), is equivalent to a sigma value (σ-point). The position of the principal stresses can be determined by locating the mean positions of σ-points, which are also intersected by GCFs for all the CIPs that produce a result. Sigma 1,2 and 3 are assigned by using motion data from slickensides and background knowledge of the geology of the area.

The advantage of Aleksandrowski's (1985) method is that it takes into account the influence of σ_2 unlike other methods. It can also be used if only limited motion data is available, with it only being required to assign the three principal stresses to the calculated locations. A problem with this method is that it is time consuming with small errors in measuring and plotting possibly resulting in discrepancies later, preventing a successful result. Also large data sets are required with no guarantee of success and no way of knowing if a data set will be successful beforehand.

4.3 RESULTS FOR M-PLANE METHOD

The fault planes that were recorded with slickensides were randomly orientated in both sampled locations (fig. 4.3). Slickenside orientation, at the location on the southwest slope of Bell Hill, was approximately along a west-northwest striking great circle. This possibly indicates that the axis of maximum compression is located in the WNW-ESE quadrant. The plotted M-planes and M-poles for this data tend to suggest a similar conclusion, with the M-poles plotting close to a south striking great circle. The main location of M-plane intersections appears to be in the WNW direction, corresponding to the location of the axis of maximum compression (σ_1)(Aleksandrowski 1985). The Great circle through the M-poles is approximately perpendicular to this orientation and would represent the plane containing the other two principal stress axes (σ_2 and σ_3). Seven M-plane common intersection points were analyzed for this population using Aleksandrowski's (1985) method. There were no GCFs located however, preventing the application of this method.

The slickenside data collected from the location on the northwest slope of Bell Hill showed no considerable uniform orientation; although most data is in the SW-NE quadrant it is very scattered. This pattern continues for the M-plane and M-pole plots with both being scattered evenly through the stereonet. It is not possible to interpret the orientation of the principal stresses from these plots as was done for the other location. There was more success with implementing Aleksandrowski's (1985) method for this data though. Ten M-plane common intersection points were analyzed. Two CIPs produced good GCFs and two others produced approximate GCFs. These approximate GCFs were assumed to be a result of errors either in data collection or plotting and are included to help support the other data.

When the σ-points and GCFs for the four analyzed populations are plotted the location of one of the principal stresses can be determined accurately in the southwest quadrant with a shallow dip (Fig.4.4). The other two principal stresses are poorly constrained with likely orientations of northwest dipping shallowly and east dipping more steeply. Assigning sigma 1,2 and 3 to the three proposed principal stresses is difficult due to the lack of data on the sense of motion. It could be assumed though that the northwest principal stress orientation is σ_1 if it is reflective

of Cenozoic deformation and the NE-SW trending structures. This would make σ_2 in the southwest orientation and σ_3 the east orientation.

This example shows the difficulties with the m-plane analysis method of Aleksandrowski (1985). The method is time consuming with no certainty of a positive result. One likely problem with the data set is the influence of Mesozoic stress regimes producing data that was difficult to differentiate from Cenozoic data. Another problem could have been the influence of normal faults forming in the thrust hanging-wall as the over steepening thrust scarp deforms under gravity. The complex nature of the internal mechanics of thrust faults, with varying shear orientations from strike-slip to normal, possibly complicates the process of the analysis more than the normal faults used in the model examples.

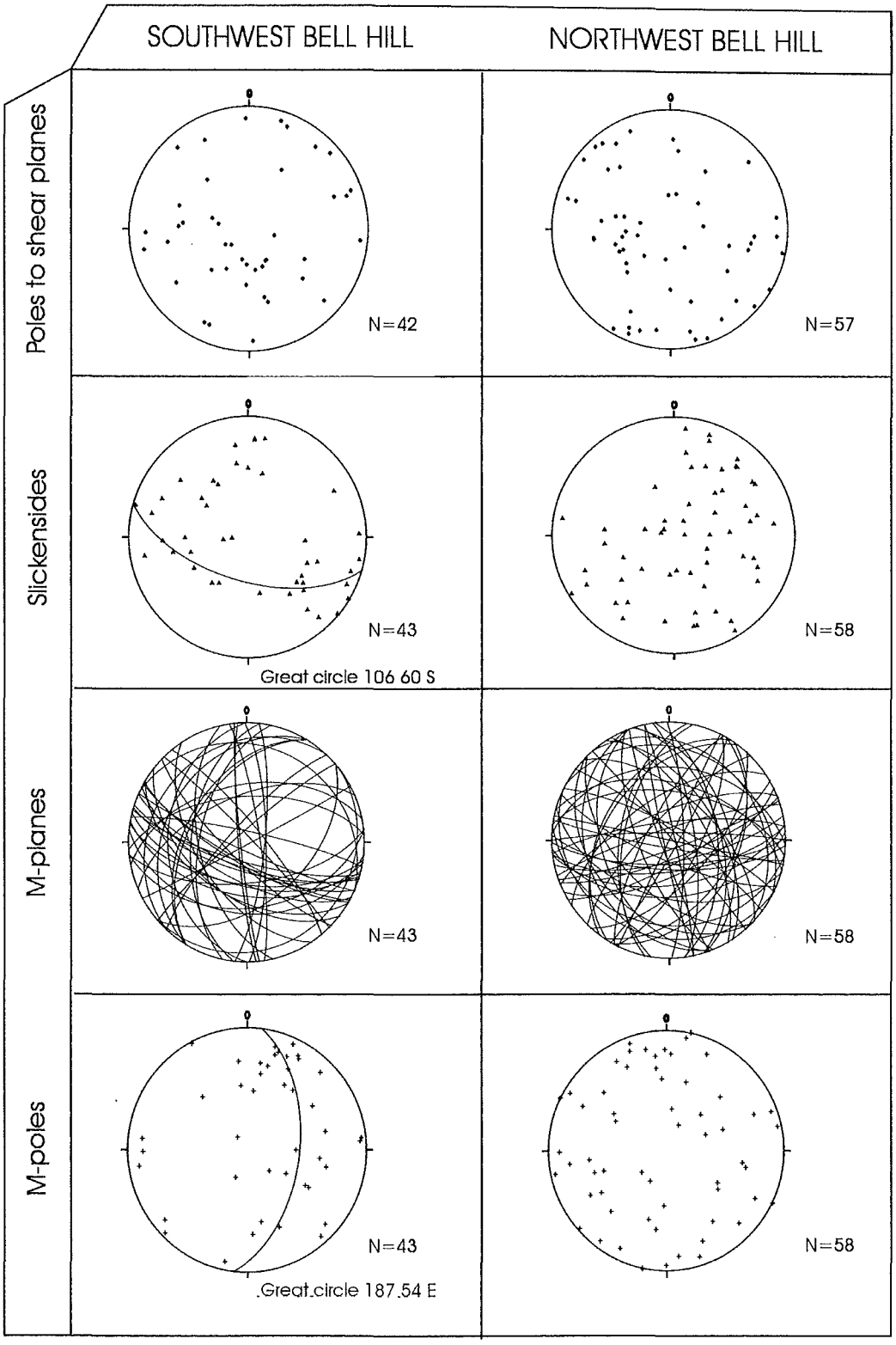

Figure 4.3. Plots of the poles to shear planes, slickensides, M-planes and M-poles for the two localities of sampling northwest and southwest Bell Hill.

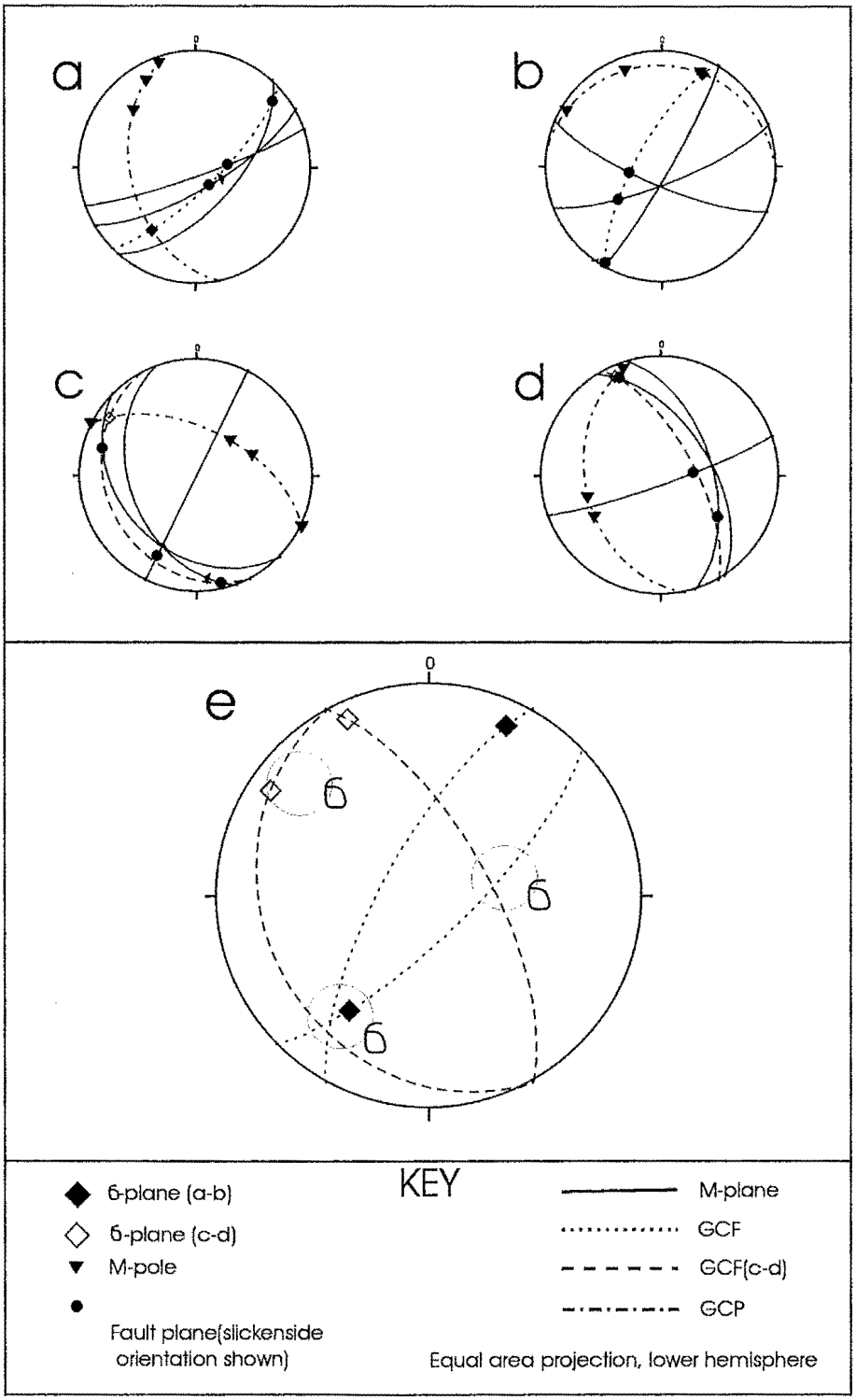

Figure 4.4. a-d are individual CIPs analyzed using Aleksandrowskis (1985) method; a and b show precise GCFs, c and d show approximate GCFs; e is the summary of the data produced by this analysis with the circles indicating locations of the principle stresses that were derived..

4.4 PT METHOD

The PT method of slickenside analysis that is installed on the StereoNett computer program was used to analyze the collected slickensides where shear motion was determined. This particular method derived after Turner (1953) is similar to the method proposed by Angelier and Melcher (1977) as cited by Mould (1992). The basis of this method is that fractures generate parallel to σ_2 with an angle of approximately 30° to σ_1. When plotted on a stereonet the pressure axis (P-axis = σ_1) is 30° from the pole to the fault along the M-plane of that fault in the direction of slip motion. The tension axis (T-axis = σ_3) is 90° from the P-axis around the M-plane. The intermediate axis (I-axis = σ_2) is 90° from the other two axes and equivalent to the M-pole to the M-plane. The same principle is used in the other method proposed by Angelier and Melcher (1977) except the angle to σ_1 is assumed to be 45° rather than 30°.

A problem with this method is that the assumption that faults form at 30° to the sigma 1 direction is only valid in ideal homogenous rocks without pre-existing fractures or shears. This is not the case with Torlesse terrane rocks. Despite this it is still possible to get meaningful results even in rocks with pre-existing fractures.

4.5 RESULTS OF PT METHOD

Slickensides with observed motions on them were rare with only nineteen recorded for the two sites. These data sets were smaller than desirable, and could have easily been biased by the lack of variation of orientations and motions that were collected. As the data sets were small the individual axes calculated for each slickenside data point are plotted as well as the averaged locations of the principal stresses calculated for the whole data set (Fig. 4.5).

Seven data points were collected from the location on the northwest face of Bell Hill. The orientation of the principal stresses calculated for the whole data set indicates a shallow dip and a northeast orientation for σ_1. When the individual data points are plotted σ_1 is not constrained so well, with an even distribution running northeast to southwest across the stereonet. The two data points indicating normal faulting are possibly representing normal

faults occurring on the hanging-wall of the thrust as it becomes over-steep. The other five points are positioned at very low dip angles. There reverse orientations can probably be explained by slight variations in their dip producing data points at either side of the stereonet. The sigma 2 and 3 points are well constrained to, with σ_2 positioned in the southeast quadrant and σ_3 positioned in the northwest quadrant.

The results for the data collected from the location on the southwest face of Bell Hill are less defined as the results already discussed for the other location. Analysis of the whole data set produces a north-northwest orientation and a moderate dip for the location of σ_1. When the individual data points are plotted there is no real trend in the distribution of any of the principal stresses. This is possibly due to the lack of an overprint on the data as appears to have occurred because of the thrust fault located at the other site of data collection. Instead here a lot of deformation is probably taken up on existing shear planes compared to the location on the northwest side of Bell Hill where new shears most likely were produced by the initiation of the thrust fault.

As mentioned above the Torlesse rocks are not the ideal example for using this method of analysis, and this possibly could have contributed to the lack of good results at the southwest Bell Hill location. It may have also been interesting to know the affect of assuming fault initiation at 30° rather than 45° to sigma 1.

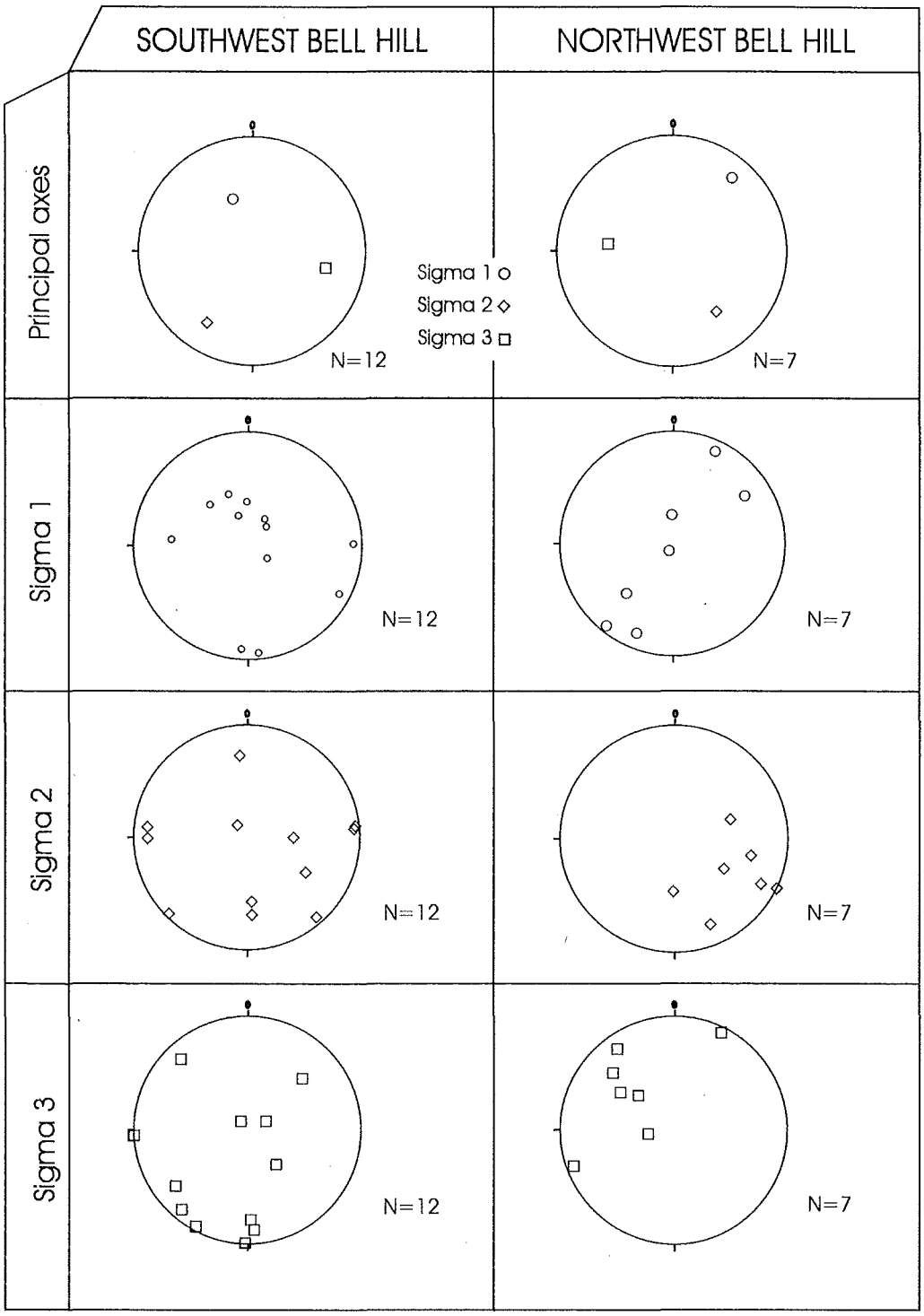

Figure 4.5. PT test results for slickensides with determined motions from the two sites of data collection; southwest and northwest Bell Hill

4.6 SUMMARY

The analysis of slickenside data from Torlesse terrane rocks to determine the stress regime operating in the study area was only marginally successful. Two orientations for sigma 1 were obtained at each location of data collection. There was no close similarity between the orientations calculated for the two locations (Table 4.1). There was however a general trend shown for a SE-NE location for sigma 1 at the northwest Bell Hill location and a general orientation in the NW quadrant for the southwest Bell Hill. The difference between the two locations is difficult to explain, but may be related to the faulting occurring on the northwest slope of Bell Hill.

The stress regime generally thought to be operating on the broad scale in North Canterbury has a sigma 1 orientation in the northwest quadrant. The value for the southwest Bell Hill location is very similar to this (Table 4.1).

Table 4.1 Summary of the results for the analysis of the slickenside data from two locations on the northwest and southwest slopes of Bell Hill using the m-plane and PT methods of analysis.

LOCATION	M-plane method	PT method
Northwest Bell Hill	SE shallow dip	NE shallow dip
Southwest Bell Hill	WNW medium dip	NNW medium dip

CHAPTER 5: GEOMORPHOLOGY

5.1 INTRODUCTION

Geomorphology refers to the features of the land and the processes that form them. The analysis of these features can prove a very valuable tool in interpreting the deformation history of a region.

The location that provided the best geomorphic history of the Springfield Fault and its related deformation in the study area was the Upper Hawkins Basin. Here qualitative analysis of terrace sequences and terrace and river gradients could be undertaken, as well as the comparison of topographic profiles across the fault scarp.

5.2 QUALATATIVE ANALYSIS OF GEOMORPHOLOGY

The geomorphology in areas of active deformation can be very easily analyzed qualitatively to get a picture of the nature of deformation that has been occurring. Rivers are especially sensitive to deformation of their channel and flood plain. Often the history of a rivers response to deformation is recorded by the abandonment or migration of channels, or by the pattern of terrace formation and down-cutting. The recorded history in the geomorphology can be interpreted to reconstruct the sequence of events that have lead to the production of the geomorphologic patterns. A relative history of deformation events can be produced allowing any subsequent absolute dating of geomorphic features to help build up a history of the absolute ages of deformation events.

Where the Hawkins River crosses the Springfield Fault the history of activity has been recorded in the terrace surfaces produced as well as in subtle changes in the rivers gradient and slope of terraces. These geomorphic features provide information as to the history and processes operating within the deformation zone of the Springfield Fault.

5.3 SCARP SEQUENCES

The history of down-cutting, and response to activity on the Springfield Fault by the Hawkins River in the Upper Hawkins Basin is well documented in the area by the

geomorphology. Three major degradation terrace surfaces are present in the basin (A-C). Two of the terrace surfaces, B and C, are displaced by the Springfield Fault, with the downstream side being uplifted. This has produced a complex history of the drainage pattern across the fault trace (Fig 5.1).

The oldest terrace surface (C) consists of three sub-terraces, a higher degraded surface on the up-thrown side of the fault, a lower more expansive surface on the up-thrown side of the fault and the surface on the down-thrown side of the fault. These surfaces date from a time when the river base-level was much higher. Drainage most likely either flowed southwest from the tributaries at the northeastern end of the basin or from the west to the east as a branch of the main river exiting along the route now occupied by the main north tributary. Reconstruction of the C terrace surface is difficult due to the limited amount of this surface left preserved.

The second oldest terrace surface (B) consists of at least five subsidiary terrace surfaces produced by displacement on the fault and local erosion of the main B terrace surface. Reconstruction of events producing these sub-surfaces indicates a complex history of erosion in response to deformation.

The main B terrace surface was a broad degradation surface occupied by the Hawkins River (Fig. 5.1). Activity of the Springfield Fault produced upthrow on the downstream side, producing the B sub-surface of maximum height (B_1). This resulted in the Hawkins River and tributaries being dammed with initial overbanking occurring. This produced erosion of the B_1 surface forming a lower B_2 surface. Following this outlets across the B_1-B_2 surface were concentrated into discrete channels, two of which are preserved. It is difficult to know if these channels formed simultaneously or progressively with abandonment following initiation of a new channel. What possibly occurred in the situation of the two preserved channels is capture of one channels flow by the other following generally simultaneous formation. These channels formed a lower terrace sub-surface B_3.

Further activity on the Springfield Fault resulted in uplift and down cutting into the B_3 surface. Some channels incised into the B_3 surface following damming of the river as a result of the fault activity were abandoned as more rapid down-cutting occurred in other

channels. These abandoned channels represent a fourth terrace subsurface B_4. The final terrace subsurface is B_5, which is the surface on the downthrown upstream side of the Springfield Fault, and the surface occupied by the youngest channels that drain this surface across the fault trace.

The younger A terrace surface is lower than the B surfaces and crosses the Springfield Fault trace without being deformed. Downstream of the fault the A surface is cut into the B surface and has cut back this surface towards and parallel to the fault trace. The B_5 sub-terrace channels grade down through the higher B surfaces onto the A terrace.

There are several factors and unknowns unrelated to the activity on the Springfield Fault that could have influenced the Geomorphology that we see at present. These include, base-level changes caused by factors other than faulting such as folding, the areas of older terrace surfaces that have been subsequently eroded, and the migration of the Hawkins River in the past.

The history of activity on the Springfield fault indicated by the geomorphology across the fault suggests two displacement events between the formation of terrace A and the time when the B terrace surface was occupied by the river. The number of events occurring in the time period between the occupation of terrace surface C and the formation of terrace surface B cannot be determined as there is not enough of the C surface still preserved. It could be expected though that there was more than one rupture event because of the size of the fault scarp.

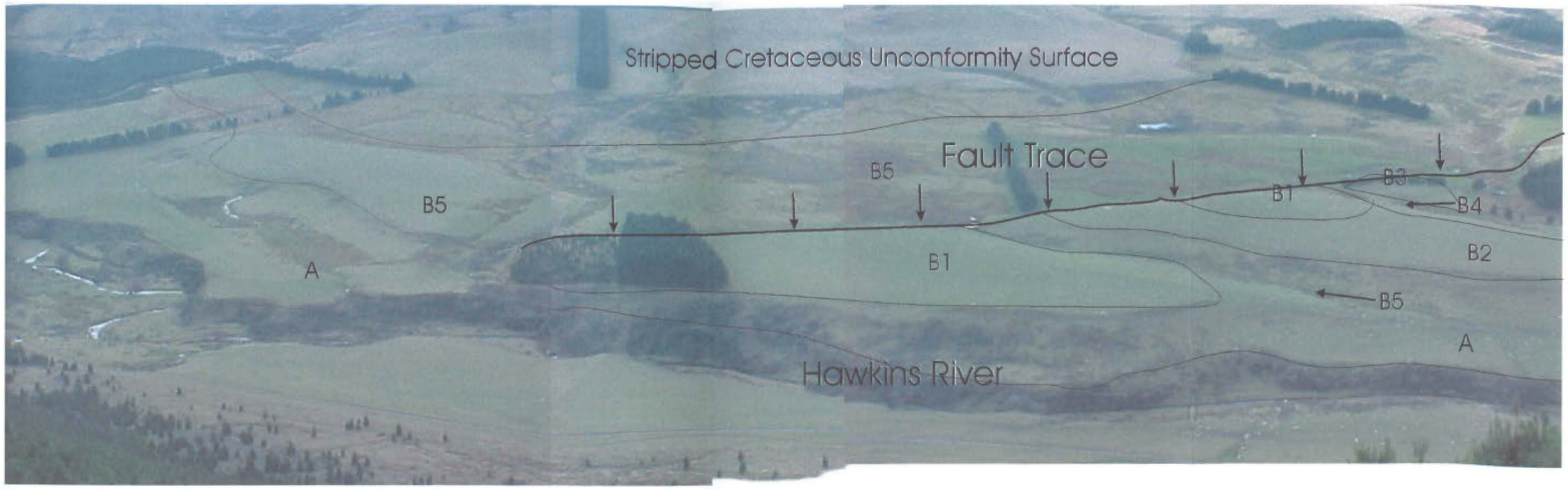

Figure 5.1. Photo of the fault trace where it crosses the Hawkins River in the Upper Hawkins Basin with the various A and B terrace surfaces discussed in the text.

5.4 TERRACE AND RIVER GRADIENTS

Rivers are especially sensitive to deformation across their channel and flood plain. Changes to a channels gradient as a result of deformation can produce aggradation or degradation in the channel or changes to the rivers bedform as the river tries to reach grade. Often active folding or faulting perpendicular to a river channel can cause the rivers bedform to change to a meandering bedform upstream of the deformation before straightening out downstream of the site of maximum uplift.

As the Hawkins River crosses the trace of the Springfield Fault it goes into a meander where the river almost turns back on itself. Upstream of this point the sinuosity of the river increases as it approaches this meander. Below the trace of the fault the river seems to straighten with much lower sinuosity. This seems to suggest that the river is responding to deformation along the fault trace. This is strange, as the terrace surface (terrace surface A) above the present surface occupied by the river is not offset by the fault.

The A terrace surface does appear to show some response to the fault trace with the formation of a swamp upstream of the fault trace. Outcrops in the terrace scarp that drops off the A surface reveal that the gravel is thicker on the upstream side of the fault trace compared to the downstream side of the fault trace, although the exact gravel basement contact upstream of the fault trace cannot be seen. This evidence combined with that shown by the current river channel tends to suggest that there has possibly been a degree of bulging or uplift along the fault trace. This must have been occurring when the river occupied the A terrace surface to account for the varying gravel thickness and must be still occurring although on a very small scale to have affected the current channel and not have affected the A terrace surface.

This warping along the fault trace is also possibly suggested by the apparent rounding of the highest B terrace subsurface (B_1). The difficulty is in knowing if this rounding is due to warping and folding or solely a result of erosion.

5.5 TOPOGRAPHIC PROFILES

Twenty-five topographic profiles were produced across the terraces and fault scarp in the Upper Hawkins Basin using an electronic distance measurer (EDM) and an electronic data logger. The aim of this exercise was to produce scarp profiles that could be morphologically analyzed (Chapter 6) and also to provide more accurate control on the dimensions and subtle changes of the morphological features.

Profiles plotted across the fault scarp show the various terrace surfaces and provide good evidence for the activity on the fault as outlined above. The B_5 surface can clearly be seen to cross over the fault trace and grade down onto the A surface on the downstream of the fault (Fig.5.2). The relative heights of the terraces are also clearly visible and the number of displacement events and the amounts of displacement can be estimated (Fig. 5.2 & 5.3).

The maximum displacement is 20.96 m between the highest C surface (C_1) and the C surface on the down-thrown side (C_2). These surfaces may not represent the same displaced surface but instead the highest C surface is more likely to be an abandoned river surface that has been uplifted. The lower C terrace surface (C_3) is possibly either the pair of the C surface on the downthrown side of the fault (C_1) or possibly a later intermediate surface between the B and C surfaces. This has displacement of 7.9 m.

The maximum displacement for the B surfaces is between B_1 and B_5 of 6.7-10 m. It appears that at least two rupture events have displaced the B surface. The most recent resulted in a vertical displacement of approximately 4.0 m. This makes the earlier one between 3 and 6 m.

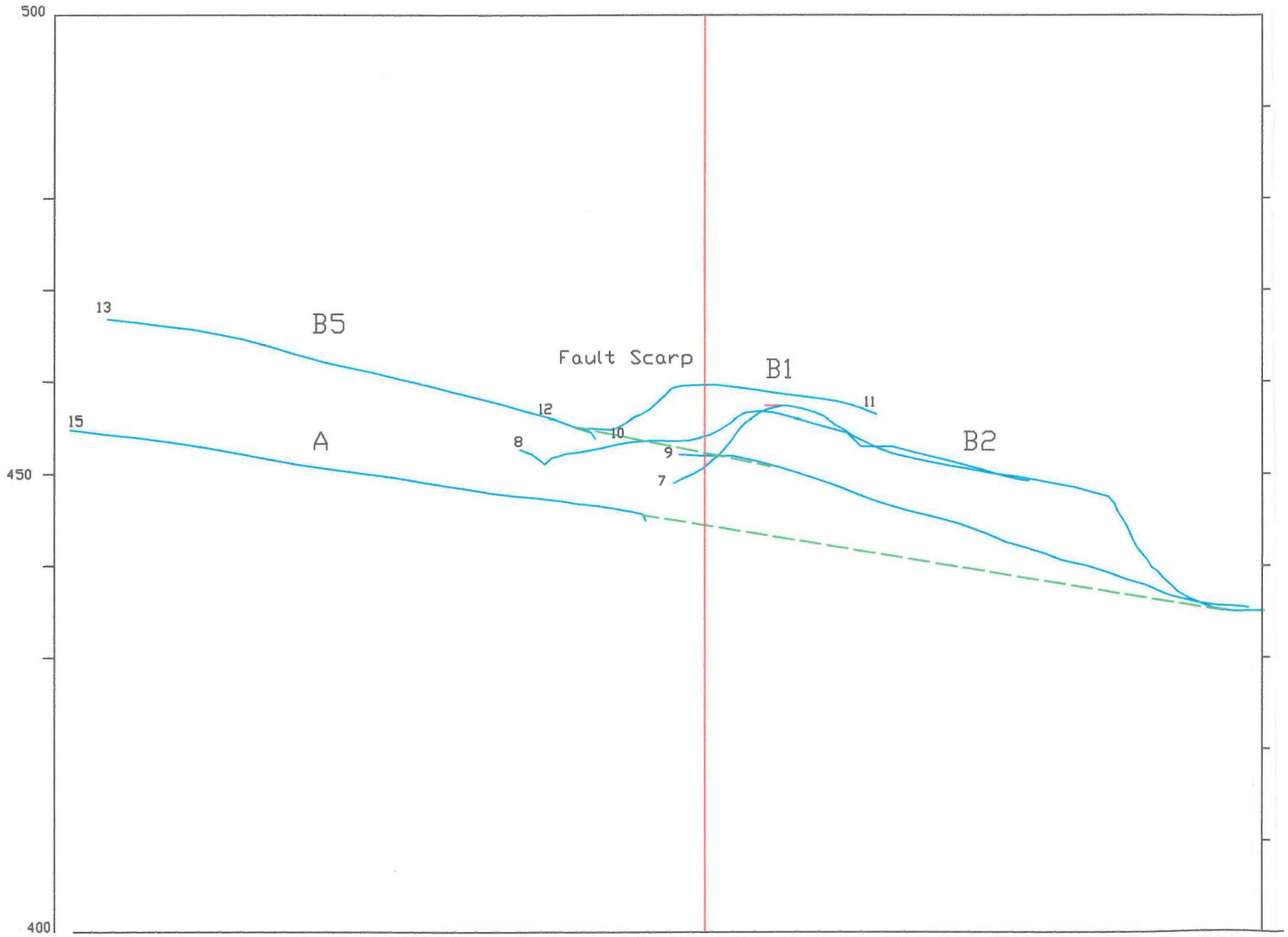

Figure 5.2. Superimposed profiles of A and B surfaces at the southern end of the fault trace in Upper Hawkins Basin measured by EDM. No vertical change, so are at relative levels. The B surfaces can be seen to grade onto the A surface. Vertical exaggeration 1:5.

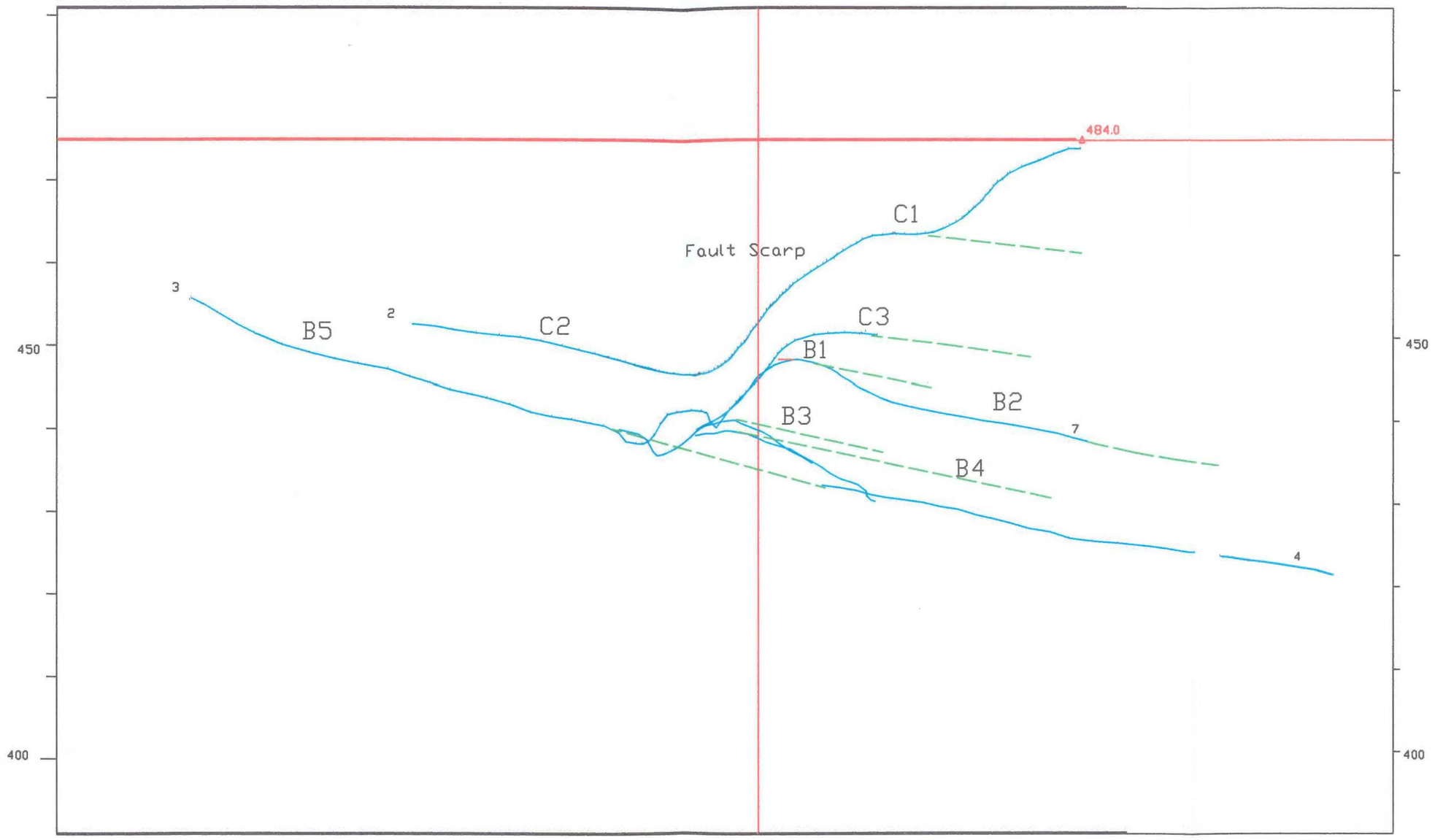

Figure 5.3. Superimposed profiles of B and C surfaces at the northern end of the fault trace in Upper Hawkins Basin measured by EDM. Vertical exaggeration 1:5.

CHAPTER 6: DATING FAULT ACTIVITY

6.1 INTRODUCTION

Dating of the activity along the trace of the Springfield Fault is reliant on interpretive techniques due to the last activity occurring prior to historical records. Radiocarbon dating of carbonaceous material, allowing rupture events to be constrained, is one of the most accurate methods of dating activity on Quaternary faults. The likelihood of locating dateable carbonaceous material in the gravels adjacent to the Springfield Fault is probably no higher than any similar site in Canterbury, despite the damming of tributaries to the Hawkins River and the formation of a swampy area. Hand auguring revealed this swamp to be reasonably shallow (1-2 m deep) with most organic material concentrated in the top 60 cm, which would allow contamination of any older material by younger material such as plant roots.

The rarity of organic material is characteristic of many gravels in North Canterbury. This is presumably the result of a dry oxidizing environment that resulted in any organic material trapped within the gravels to decompose, not being preserved. As a result other methods of dating have often been implemented.

Weathering rind dating (Chinn 1981; Whitehouse *et.al.* 1984) is one such method that has often been used, with varying success in Canterbury (Garlick 1992; Mould 1992). The river terraces and fans displaced by the fault trace are generally sparse in exposed Torlesse boulders across their surfaces making this method largely unfeasible.

Morphological analysis of the degradation of fault or river-cut terrace scarps is a method of quantitatively determining the ages of different scarps, and also can provide approximate absolute ages of Holocene scarps.

6.2 ANALYSIS OF SCARP MORPOLOGY

A major part of this study is to determine the applicability of morphological analysis of scarps in dating fault activity in the tectonic and environmental setting of Canterbury. Most analysis of scarp degradation in the literature is from arid environments, due to the

lack of organic material for radiocarbon dating and the reduced influence of vegetation on scarp degradation. Despite the contrast in environment, in the wetter and well-vegetated central Canterbury foothills, the same principles used in other analyses of scarp morphology should stand as long as all factors between scarp sites are equal and climatic conditions have not varied greatly during the Holocene.

6.3 THEORY OF MORPHOLOGICAL ANALYSIS

Scarp development in cohesionless materials begins with a gravity-controlled phase of slope decline reducing the scarp to the angle of repose for the material, generally of 30-35° for alluvium or soil. This is a rapid process lasting for approximately 10-100 years. Slower erosional processes such as slope wash and rain splash then become dominant, rounding the angularities at the base and crest of the scarp reducing the maximum scarp slope. Morphological dating methods have developed from the simple observation that the shape of a scarp is the function of its age. The maximum scarp slope and the curvature of the crest are suggested to be age dependent.

The diffusion model of scarp degradation (Avouac 1993; Avouac *et al.* 1993; Hanks 2000) uses the idea of the maximum scarp slope. By calculating the rate of the down slope transfer of material and reduction of the maximum slope, which is time dependent. Conservation of mass on the scale of the scarp is assumed allowing the assumption that erosion from the top half of the scarp is equal to the amount of deposition occurring on the bottom half of the scarp. The erosional diffusion equals the depositional diffusion allowing a spatially constant, mass diffusivity constant (κ) to be assumed

The difficulty in the use of this and other methods is that the calculated diffusion age equals the mass diffusivity constant multiplied by the absolute age of the scarp. This means to determine the absolute age of the scarp the mass diffusivity constant is needed. This is difficult to determine, and can vary greatly, by up to a factor of ten (Avouac 1993), even between scarps formed in similar materials and under similar environmental conditions. Mass diffusivity is considered to vary between 0.7 and 5.2 m^2 /kyr for scarps 10-15 m high and between 0.3 and 1.6 m^2 /kyr for scarps about 5 m high indicating a positive correlation between scarp height and mass diffusivity (Avouac 1993). Generally a

scarp of known age is needed in the same area to calibrate the absolute ages of other scarps.

6.4 MORPHOLOGICAL ANALYSIS OF SCARP PROFILES

Twelve topographic profiles were produced across the fault scarp in the Upper Hawkins Basin using electronic distance measurement (EDM) equipment. A further seven profiles were produced across the river terrace scarp between the A and B terraces. Morphological dating models could then be applied to these profiles. The terrace scarps would allow a minimum age of the last deformation to be calculated, while the fault scarps would provide a direct age of activity.

A simple spreadsheet program (formulated by Dr. J. Mckean) using the principles outlined above was used to analyze the two best fault scarp profiles and the best river terrace profile. The profiles were selected for smoothness and best fitting to an ideal scarp profile, which has had equal erosion and deposition. The program simply calculates the diffusive flux (γ) by multiplying the slope of an increment of the profile ($\delta u/\delta x$) by a constant, the diffusivity (κ) (m^2kyr), which is a value unknown that is assigned a value (equation 1). The change in elevation with time of the increment of the profile ($\delta u/t$) is then calculated by calculating the net accumulation and erosion from the diffusive flux entering the increment of profile from above (γa), minus the diffusive flux exiting the increment of profile going down slope (γb) (equation 2).

$$\text{Equation 1} \quad \gamma = (\delta u/\delta x)\kappa$$

$$\text{Equation 2} \quad \delta u/t = (-\gamma b + \gamma a)/\delta x$$

The change in elevation with time can then be subtracted from the current profile, in effect going back in time, creating a theoretical profile of what the scarp would have looked like one thousand years earlier. Continuing to subtract the elevation change with time from the calculated profiles, reconstructing the process of degradation until the profile closest to fitting that of a pristine scarp is constructed meaning the age of the scarp is equal to the number of times the elevation change with time had to be added to the profile multiplied by 1000 years.

Of the nineteen profiles that were measured the three that best fitted a model degraded scarp (Fig. 6.1) were analyzed using this method. They were two fault scarp profiles (profiles 11 &17) and one profile across the A terrace surface riser (profile T1).

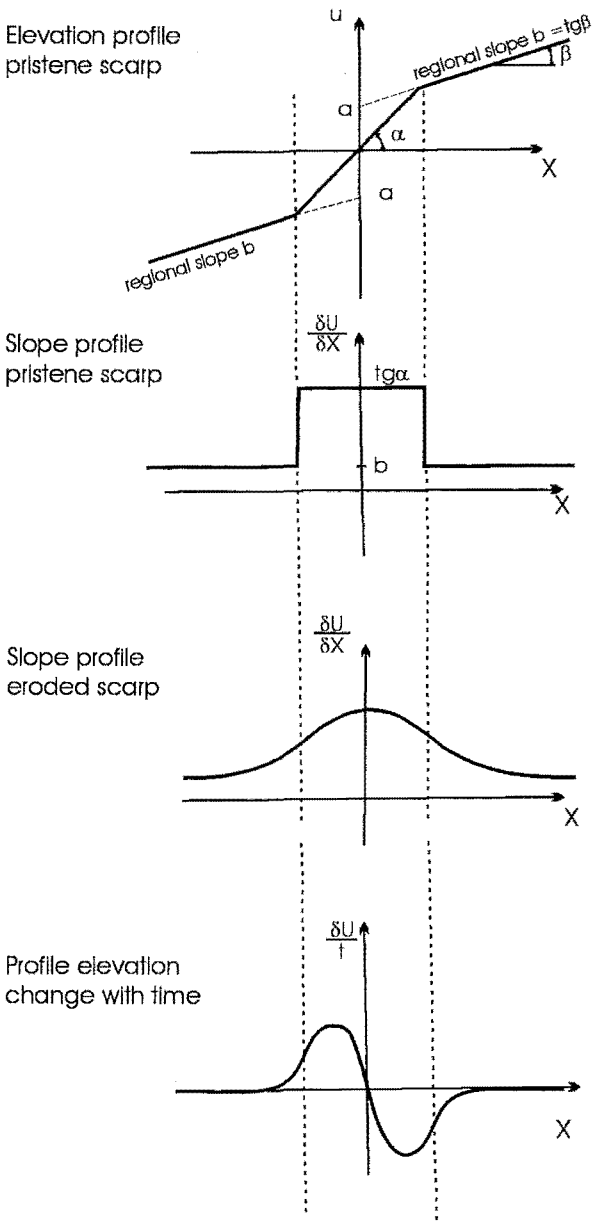

Figure 6.1. Simple approximation of fresh scarp morphology. It represents a scarp offseting a planar regional surface once gravitational collapse of free face has stopped. α is angle of repose, *b* is regional slope,and *a* is half offset. Slope profiles for fresh and eroded scarps are shown underneath. At the bottom the profile of the elevation change with time is shown. *U* is vertical distance, *X* is horizontal distance, *t* is time, and *tg*α is the initial scarp slope.

6.5RESULTS OF MORPHOLOGICAL ANALYSIS

Morphological analysis of the scarps was not as successful as was hoped. This was most likely due to the nature of the scarps which where not as smooth and well fitted to a model scarp as first observed.

Profile 11 (Fig. 6.2) had several features inhibiting analysis. The first is the fact that the regional slope dips into the fault scarp (Fig. 6.2A). This creates problems with modeling at the top of the scarp as the steepest point of the scarp occurs near its top rather than in the middle as assumed by the model. Another problem is that the slope along the scarp is variable (Fig.6.2B), not forming a smooth curve as in the model curve for slope versus distance across a scarp(Fig 6.1). This causes problems with the values calculated for diffusivity flux, and therefore the predicted elevation changes in points along the scarp (Fig.6.2C). An example of the variations in the slope is the small indent near the top of the scarp where the slope is 0% (Fig. 6.2A,B). This is possibly an indication of the point of breakout for the most recent rupture along the fault.

Profile 17 (Fig.6.3) is a better fit to the model with a slope versus distance graph showing an approximate match to the model curve (Fig. 6.3B). The calculated elevation change with time, versus distance (Fig. 6.3C), is again slightly scattered around the critical area and shows the reverse pattern to what we would have expected. Instead of net elevation loss at the top of the scarp and net elevation gain at the foot of the scarp the reverse is occurring. This is possibly a result of the steepness of the regional slope that has caused the change in slope between points to be smaller and therefore more sensitive to local variations in the profile of the scarp. There appears to be a slight convex portion in the profile at the top of the scarp and a slight concave portion near the base of the scarp. These very subtle features are responsible for causing the highest values of elevation change and distorting the data.

The roughness of these profiles is probably due to rills and uneven areas created by factors varying spatially other than those involved in two-dimensional degradation of a scarp profile. Inaccuracies occurring during profile measurement are likely to be small and not significant compared to the general topographic variations.

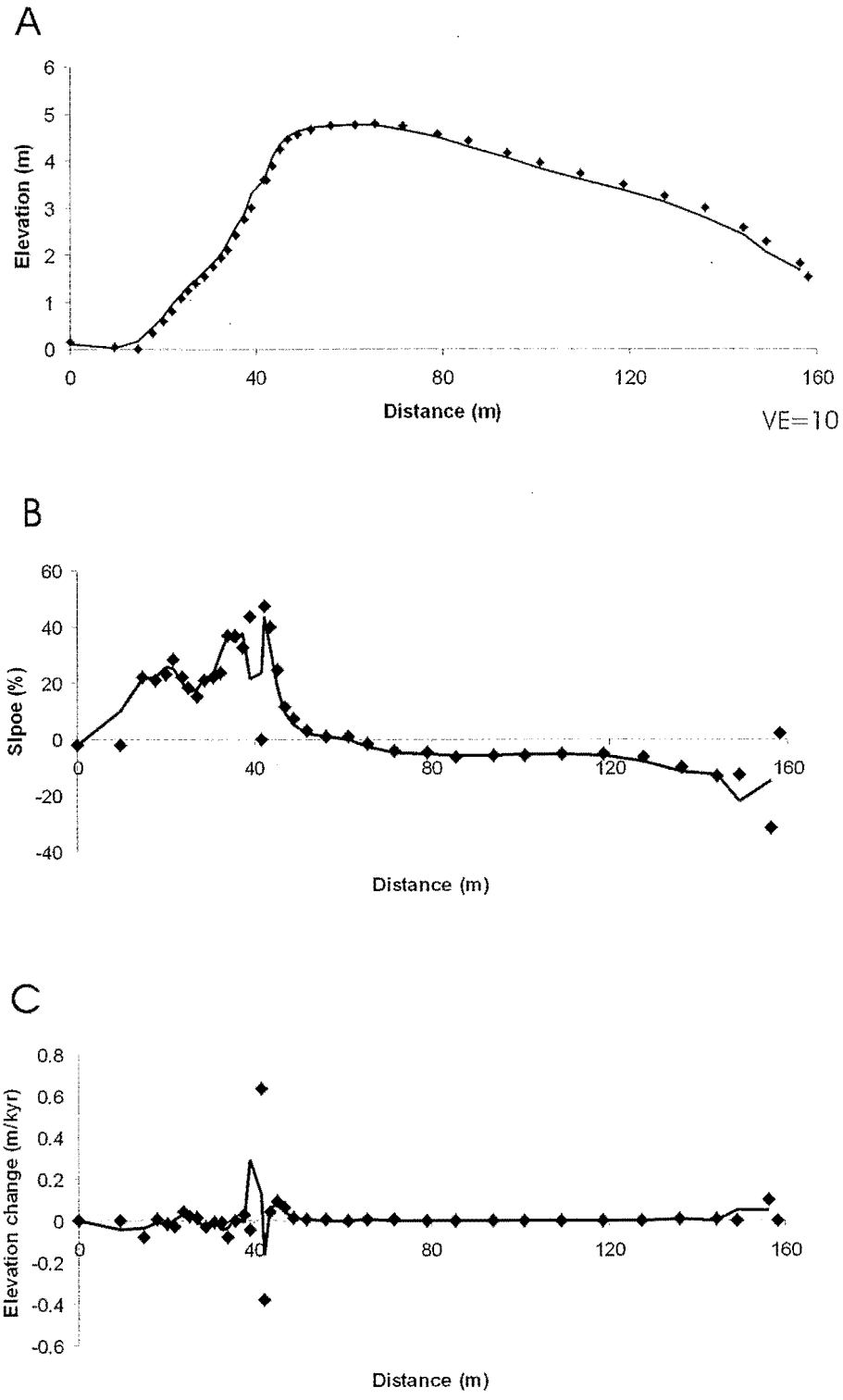

Figure 6.2 A, shows a profile (profile 11) across the fault scarp with vertical exaggeration of 10 times. B, shows the slopes measured between points on the profile. C, is a plot of the calculated change in elevation using the spreadsheet program for morphological dating of the fault scarp (diffusivity = 2m2/kyr). Solid lines on graphs are best fit lines formed by averaging two adjacent points.

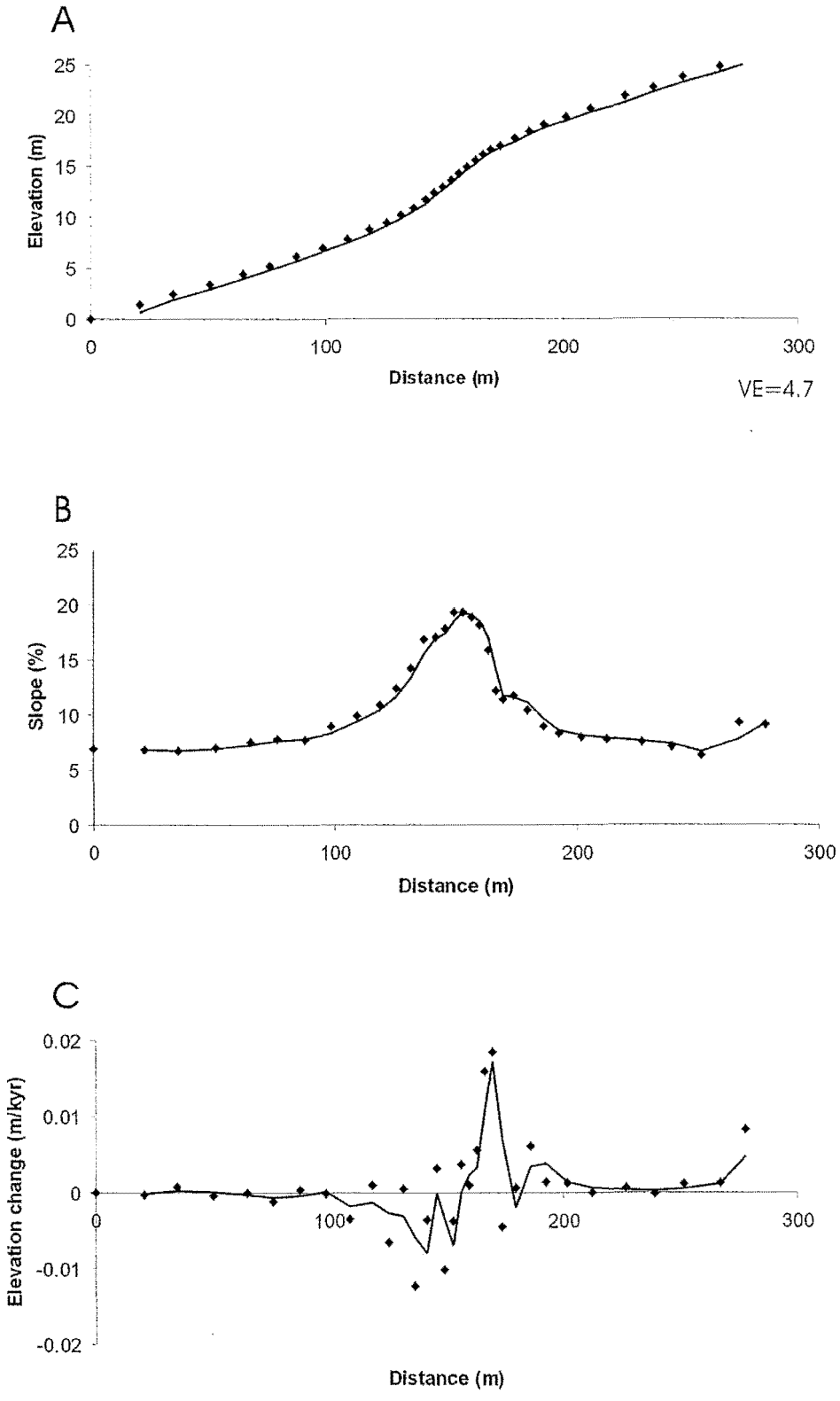

Figure 6.3. A, shows a profile (profile 17) across the fault scarp with 4.7 times vertical exaggeration. B, shows the calculated slopes between points on the profile. C, is the plot of the calculated change in elevation per thousand years as calculated using the spreadsheet program for morphological dating of the scarp (diffusivity = 1.6m2/kyr). Solid lines on graphs are best fit lines formed by averaging two adjacent points.

Profile T1, again does not show the accurate fitting to the model scarps that is necessary to have successful modeling (Fig. 6.4). This is however probably the best of the three analyzed scarps. The calculated elevation change with time (Fig. 6.4) shows a general similarity to the model scarps but closer inspection reveals that certain points of the scarp have calculated elevation changes that we would not expect, but can be averaged out in analysis.

The profile T1 was the only one of the three profiles analyzed that produced a good result (Fig. 6.5). Even this was not ideal. A difficulty was that there was no known measurement of diffusivity so it involved calculating an age for an estimated diffusivity rate and multiplying the two together to get a degradation age of 5200. The best fit for the initial scarp profile was not as good as hoped, but the plot of the slope of points (Fig. 6.5) is the best fit to the model for a newly formed scarp that could be estimated. To determine the absolute age of the scarp the rate of diffusivity is required, which must be calculated from scarps with measured absolute ages that have been morphologically analyzed. Using the ranges of diffusivity rates for a 10-15 m scarp suggested by Avouac (1993) of between 0.7 and 5.2 m^2/kyr the range of age for the scarp is 7500-1000 yrs. These values come from arid conditions meaning that diffusivity could be higher here due to greater rainfall.

The problem with this model is that we are substituting in a value for the rate of diffusivity meaning that absolute dating is not possible. Diffusivity is also very variable as noted above, varying with scarp height and presumably also with climate. It is also impossible to compare the age values for scarps calculated assuming the same diffusivity, unless they are of similar height, because diffusivity varies with scarp height.

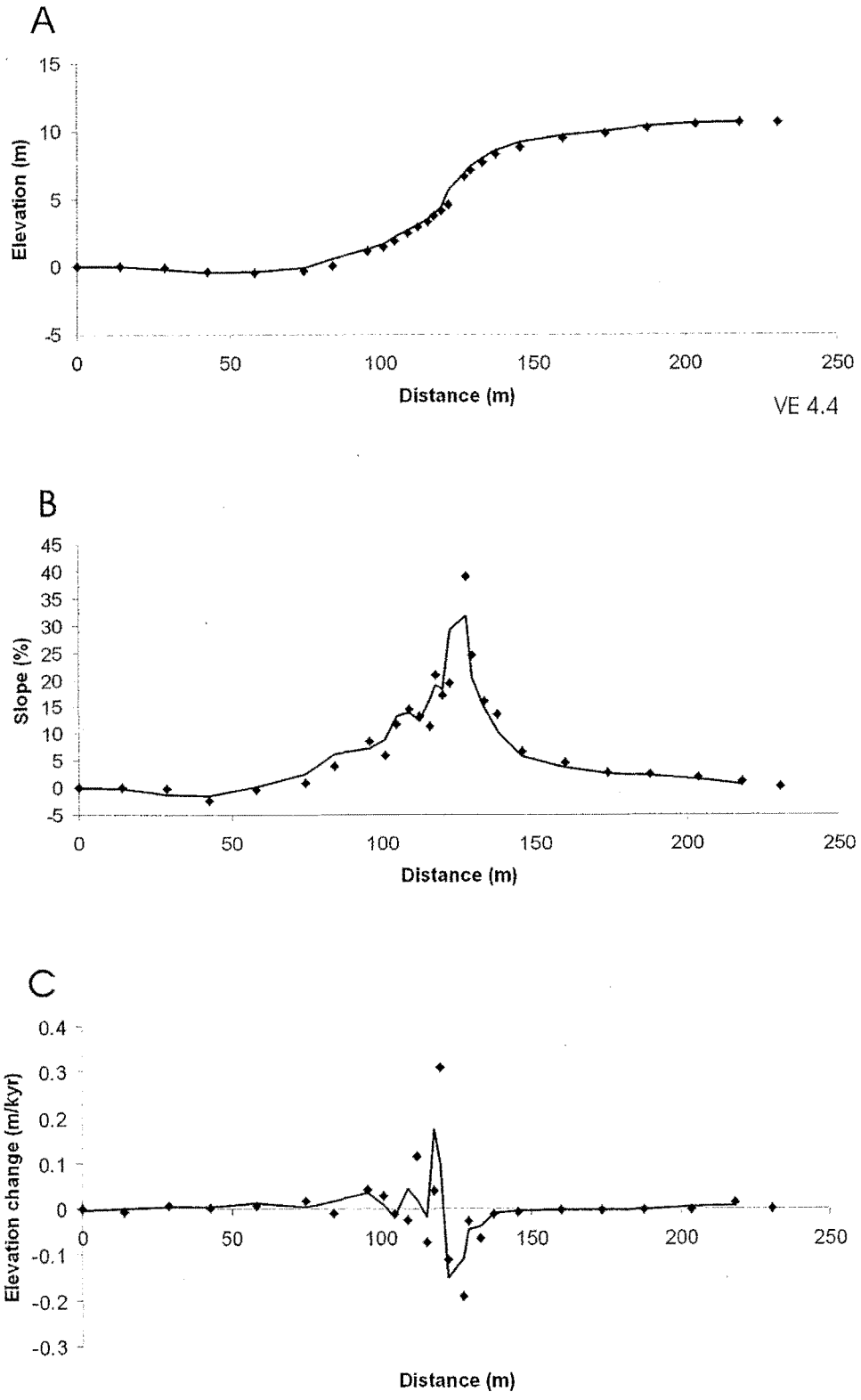

Figure 6.4 A, shows a profile across the A terrace surface riser (profile T1)with vertical exaggeration of 4.4 times. B, shows the calculated slopes between points on the profile. C, is the plot of the calculated change in elevation per thousand years as calculated using the spreadsheet program for morphological dating of the scarp (diffusivity =4m2/kyr). Solid lines on graphs are best fit lines formed by averaging two adjacent points.

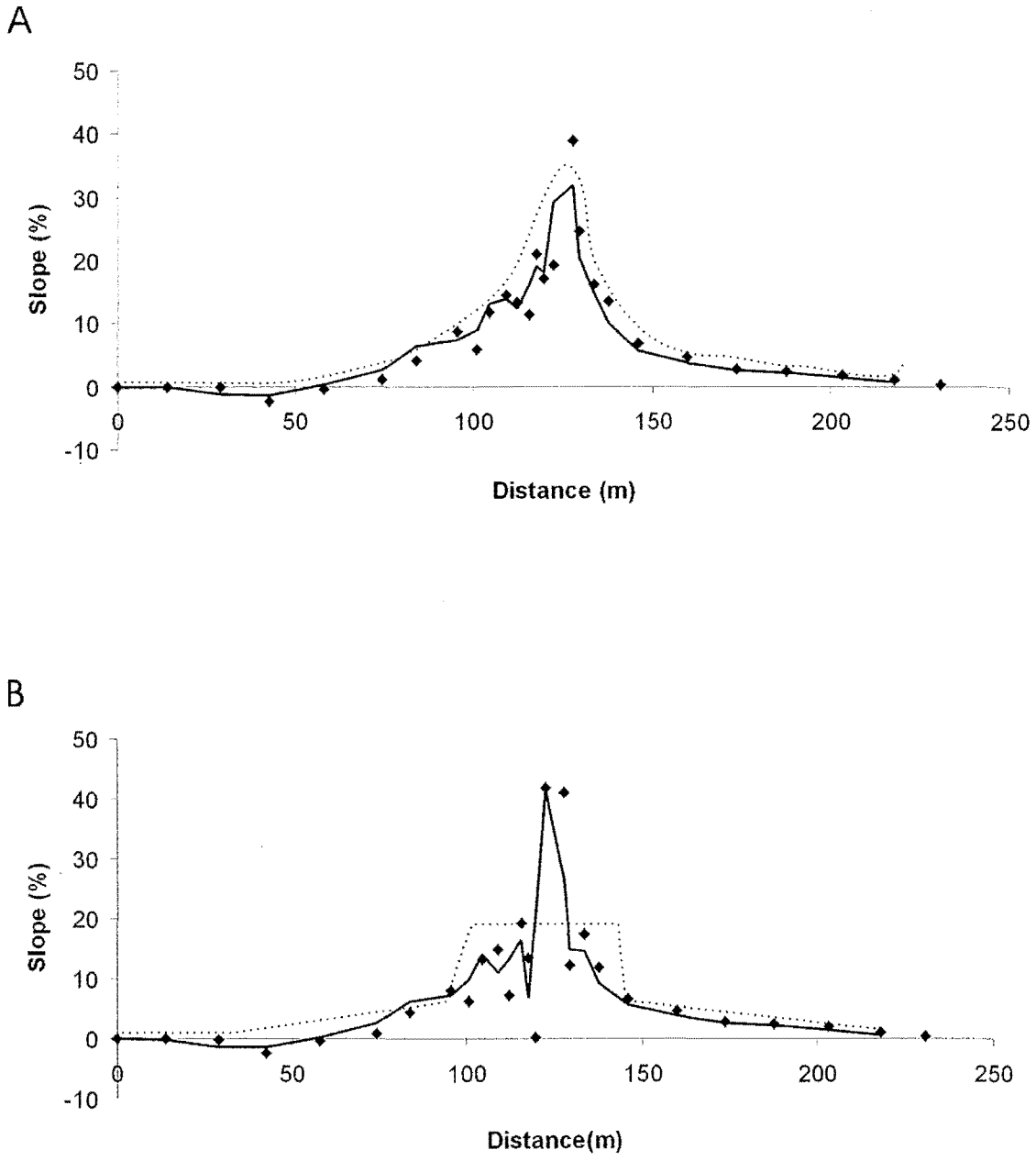

Figure 6.5. A, the slopes between points on the terrace riser of terrace surface A at time 0 (measured profile). B, shows the analyzed slope data which is assummed to be the best fit for the scarp at time of initiation that could be achieved by using the model outlned in the text. Degradation age (Diffusivity X absolute age) = 5200. Dotted lines indicate sketched lines showing the difference in the degraded profile (A) and best fit newlyformed scarp (B).

6.6 RECOMMENDATIONS FOR MORPHOLOGIC DATING OF SCARPS

The most important consideration when attempting to date scarps by their morphologic features is selection of the right profiles across a scarp. The profile of the scarp must fit well to a theoretical shape of a degraded scarp with no major deviations in slope caused by rills or activity by animals. Sites selection for surveying profiles is therefore important making sure that any areas where the profile has been altered are avoided.

Before morphologic dating can become an effective tool a large database of diffusivity rates is required. This requires that scarps of known absolute age be profiled and analyzed morphologically to obtain diffusivity rates that can be used for scarps of unknown age. Until then morphologic dating is still a useful method to apply in conjunction with other methods to support the ages calculated by those methods. In this situation the diffusivity rate is what is being calculated rather than the absolute age.

CHAPTER 7: CONCLUSIONS

The Springfield Fault is a southeast dipping thrust fault that is more than likely associated with the Kowai fault to the north and its associated hanging wall anticline the Russell Range. The trace of the Springfield Fault is most prominent in the Upper Hawkins Basin where it displaces river terraces as it crosses the Hawkins River. The fault produces a small fault-controlled outlier of younger Cretaceous Broken River Formation within Russell Range's predominating Triassic Torlesse terrane rock type. The fault trace cannot be traced very much further towards Springfield than the saddle dividing the Upper Hawkins Basin from the north facing slopes of the Russell Range. At this point it is suspected that the fault splays possibly as a result of interference from the Kowai Fault. These splays cannot be traced but presumably follow several prominent streams out towards the Kowai River Valley and Springfield.

Analysis of the stress regime in the basement Torlesse rocks, by the use of slickenside orientation measurements revealed a general NW-SE to NE-SW direction for the principal axis of compression from the m-plane and PT methods. The bedding appeared to be folded around fold axes that strike approximately NW-SE.

Analysis of the geomorphology of the fault trace as it crosses the Upper Hawkins Basin produces a good chronology of river terrace offset and the rivers response to activity along the fault trace. This allowed a history of activity on the fault to be established. At least two ruptures on the fault have occurred since the river occupied the terrace surface assigned as B surface and the abandonment of terrace surface assigned A. These displacements were of the order of 3-4 m each time.

An attempt to date the age of scarps from their morphology was made. Three scarp profiles were analyzed in the end, two of the fault scarp and one of river terrace A. The profiles across the fault scarp failed to produce any result of degradation age, as their profile was too uneven, with subtle changes in scarp slope affecting the results. A result

for the river terrace scarp was obtained. A degradation age of 5200 years was calculated equaling an absolute age of between 1000 and 7500 years.

Two difficulties were discovered for methods of morphologically dating scarps. The first is that the scarps have to be smooth without deviations from a slope profile of a model curve. This is very difficult to achieve as animals or the formation of rills can easily affect scarps.

The second difficulty is that any morphological dating method can only calculate the degradation age of the scarp which is the diffusion rate multiplied by the absolute age. This means that the degradation rate must be known to calculate an absolute date. The degradation rate can vary spatially with the height of the scarp and with time. It is necessary then to sample a number of terrace profiles and have some sort of age control on at least one profile so that the diffusion rate can be calculated. It is important for getting this method running in New Zealand that morphological analysis is undertaken on scarps that have absolute ages known so that a data base of diffusion rates can be built up and relationships for diffusion rates versus scarp height be developed.

7.1 FUTURE WORK

The future work recommended for developing the idea of morphological dating of scarps is largely outlined above, and generally involves the absolute dating of scarps to build up a database, but also the application of the method to scarps that are suitable.

Further work is also needed in the area surrounding the this study area including the Kowai Fault, the Thirteen Mile Bush area to the west and the High Peak Valley to the south. Work in the High Peak Valley would help to determine if the Springfield Fault continues into this area or if new structures develop and if the glacial history of the valley involved the Upper Hawkins Basin.

REFERENCES

Aleksandrowski, P. 1985. Graphic determination of principal stress directions for slickenside lineation populations; an attempt to modify Arthaud's method. *Journal of Structural Geology* **7** 73-82

Andrews, P. B., Speden, I. G., Bradshaw, J. D. 1976. Lithological and paleontological content of the Carboniferous-Jurassic Canterbury Suite, South Island, New Zealand. *N. Z. Journal of Geology and Geophysics* **19.6** 791-819.

Andrews, P. B., Field, B. D., Browne, G. H., McLennan, J. M. 1987. Lithostratigraphic nomenclature for the Upper Cretaceous and Tertiary sequence of Central Canterbury, New Zealand. *New Zealand Geological Survey record 24.*

Angelier, J. and Mechler, P. 1977. Sur une méthode graphique de recherché des constraints principles également utilizable en tectonique et en séismologie: la méthode des diédres droits. *Bull. Soc. Géol. Fr.* **19,** 1309-1318.

Arthaud, F. 1969. Méthode de determination graphique des directions de raccourcissement, d'allongement et intrmédiaire d'une population de failles. *Bull. Soc. Geol.. Fr. 7 Sér.* **11.** 729-737

Avouac, J. P. 1993. Analysis of scarp profiles: Evaluation of errors in morphological dating. *Journal of Geophysical Research.* **98 B4**, 6745-6754

Avouac, J. P., Tapponnier, P., Bai, M., You, H., Wang, G. 1993. Active thrusting and folding along the Northern Tein Shan and Late Cenozoic rotation of the Tarim relative to Dzungaria and Kazakhstan. *Journal of Geophysical Research.* **98 B4**, 6755-6804

Bradshaw, J. D., 1971. Stratigraphy and structure of the Torlesse Supergroup (Triassic-Jurassic) in the foothills of the Southern Alps near Hawarden (S60-61), Canterbury. *N. Z. Journal of Geology and Geophysics* **15.1** 71-87.

Bradshaw, J. D., Adams, C. J., Andrews, P. B. 1980. carboniferous to Cretaceous on the Pacific margin of Gondwana: The Rangitata Phase of New Zealand. *Proceedings of the Fifth International Gondwana Symposium ,Wellington , New Zealand.* pp.217-221

Brown, L. J. and Wilson, D. D. 1988. Stratigraphy of the late Quaternary deposits of the northern Canterbury Plains, New Zealand. *N. Z. Journal of Geology and Geophysics.* **31.** 305-335.

Bull W. B. & Cooper A. F. 1986. Uplifted marine terraces along the Alpine Fault, New Zealand. *Science* **234,** 1225-1228.

Chinn, T. J. 1981. Use of rock weathering rind thickness for Holocene absolute age dating in New Zealand. *Arctic and Alpine Research.* **13,** 33-45

Cox S. H., 1884. On the Springfield Colliery. *Report Geological Survey.* pp.19-22.

---------- 1884. On Mt. Somers and Malvern Districts. *Report Geological Survey.* pp.22-45.

---------- 1886. On the Springfield Colliery. *Report Geological Survey.* pp. 22-25.

Coyle, S. A. 1988. The Porters Pass Fault. Unpublished M.Sc. thesis held by the University of Canterbury Library.

De Mets, C., Gordon, R. G., Argus, D.F. and Stein, S. 1990. Current plate motions. *Geophysical Journal International* **101.** 425-478.

Garlick, R. D. 1992. Lees Valley Fault, North Canterbury. Unpublished B.Sc (Hons) dissertation, University of Canterbury Library.

Hanks, T. C. 2000. The Age of Scarplike Landforms from Diffusion-Equation analysis. *In.* Quaternary Geochronology: Methods and Applications. American Geophysical Union.

Hector, J. 1871. On the geological structure of the Malvern Hills District. *Report Geological Survey* pp. 46-55.

Lindop A. B. 1886. Malvern Hills Coal-mines. *Report Geological Survey.* pp.15-21.

---------- 1886. On the Springfield Colliery. *Report Geological Survey.* pp.25-27.

Marden, M. 1976. Late Pleistocene geology of the Kowai River Valley, mid-Canterbury. Unpublished M.Sc. thesis held by the University of Canterbury library.

Mould, R. 1992. structure and Kinematics of the Late Cenozoic deformation along the Western Margin of the Culverden Basin, North Canterbury, New Zealand. Unpublished M.Sc. thesis held by the University of Canterbury library.

Nicol, A., Wise, D. U. 1992. Paleostress adjacent to the Alpine Fault of New Zealand: Fault, vein, and styolite data from the Doctors Dome area. *Journal of Geophysical Research.* **97, B12,** 17685-17692

Norris, R.J., Koons, P.O. and Cooper, A.F. 1990. The obliquely-convergent plate boundary in the South Island of New Zealand: Iplications for ancient collision zones. *Journal of Structural Geology* **12** 715-725.

Rains, R. B. 1967. The late Pleistocene glacial sequence of the High Peak valley, Canterbury. *N. Z. Journal of Geology and Geophysics.* **10.**

Speight R. 1924. The Benmore coal area of the Malvern Hills. *Trans. N.Z. Inst.* Vol55, pp. 619-26.

---------- 1928. The geology of the Malvern Hills. *New Zealand department of Scientific and Industrial Research geological memoirs* **1.** 72p

Turner, F. J. 1953. Nature and dynamic interpretation of deformation lamellae in calcite of three marbles. *Am. J. Sc.* **251,** 276-298

von Haast J. 1871. Preliminary report on the Malvern Hills, Canterbury. *Report Geological Survey.* pp. 135-46.

---------- 1872. Report on the Geology of the Malvern Hills. *Report Geological Survey.* pp.1-85

Whitehouse, I. E., McSaveney, M. J., Knuepfer, P. L. K. and Chinn, T. J. 1986. Growth of weathering rinds of Torlesse sandstone, Southern Alps, New Zealand. *In.* Colman, S. M. and Dethier, D. P., *eds.* Rates of Chemical weathering of rocks and minerals. Academic Press.

Wibberley, C. A. J. 1997. Three-dimensional geometry, strain rates and basement deformation mechanisms of thrust-bend folding. *Journal of Structural Geology.* **19,** 535-550

Wilson, D. D. 1988. Quaternary geology of northwestern Canterbury Plains (Sheet L35 and parts sheets L36, M35, & M36) 1:100 000. New Zealand Geological Survey miscellaneous series map 14. Map (1 sheet) and notes. Wellington, New Zealand. Department of Scientific and Industrial Research.